JCTC Journal of Chemical Theory and Computation

Article

pubs.acs.org/JCTC

Ab Initio Calculation of the Ultraviolet–Visible (UV-vis) Absorption Spectrum, Electron-Loss Function, and Reflectivity of Solids

Anna Maria Ferrari,*[,†] Roberto Orlando,[†] and Michel Rérat[‡]

[†]Dipartimento di Chimica IFM, Università di Torino and Nanostructured Interfaces and Surfaces (NIS)—Centre of Excellence (http://www.nis.unito.it), Via P. Giuria 7, 10125 Torino, Italy

[‡]Equipe de Chimie Physique, IPREM UMR5254, Université de Pau et des Pays de l'Adour, 64000 Pau, France

Supporting Information

ABSTRACT: The field frequency has recently been taken into account in the coupled-perturbed Hartree–Fock or Kohn–Sham method implemented in the CRYSTAL code for calculating the high-frequency dielectric constant of semiconductors up to the first electronic transitions. In this work, we document how the code has been generalized and improved in order to compute the full ultraviolet–visible (UV-vis) absorption spectrum, the electron loss function, and the reflectivity from the real and imaginary parts of the electric response property. We show how spectra are modified when the crystalline orbital relaxation due to the dynamic electric field is taken into account, and how this modification increases with the percentage of Hartree–Fock exchange in the unperturbed hybrid Hamiltonian.

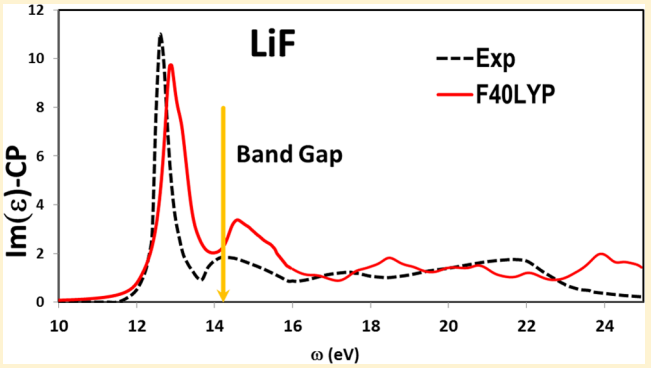

INTRODUCTION

The coupled-perturbed Hartree–Fock (CPHF) method[1] at first order of perturbation has been implemented a few years ago in the CRYSTAL code[2] for calculating the electronic contribution to the so-called high-frequency polarizability (or ϵ^{∞} dielectric constant) of closed- and open-shell periodic systems. The CRYSTAL[3,4] code, which uses atomic orbitals (AOs) for building Bloch functions (BF), solves the Hartree–Fock (HF) and Kohn–Sham (KS) equations, the latter with different types of hybrid Hamiltonians in the framework of the density functional theory (DFT). As a result, the coupled-perturbed method has been adapted at the first and second orders of perturbation for the KS equation.[5] More recently, the ω-frequency of the field has been introduced in the CPHF(KS) method, to allow study of the real part of $\epsilon^{\infty}(\omega)$, or of the refractive index n ($n = (\epsilon^{\infty})^{1/2}$), as a function of the light wavelength.[6] Applications to the photoelastic tensor and its dependence on frequency is described in refs 7 and 8.

Near resonance, the dielectric response, which is related to second-order transition amplitudes due to a time-dependent electric field perturbation, is a complex function that is dependent on a damping factor related to the finite lifetime of excited states, which, depending on several physical interactions in solids (phonon coupling, defects, ...), is not easy to evaluate. The imaginary part of $\epsilon^{\infty}(\omega)$ leads to the ultraviolet–visible (UV-vis) spectrum, i.e., the oscillator strengths versus transition or pole energies. In the following section, we show how it is computed in the full range of UV–vis energies for periodic systems, by slightly modifying the frequency-dependent CPHF(KS) method already implemented in the CRYSTAL code. The performance of the method, similar to the time-dependent Hartree–Fock (TDHF) method[9] or to the configuration interaction singles (CIS) method[10,11] as implemented in a molecular context, or to the time-dependent DFT (TDDFT) and equivalent Bethe–Salpeter equation (BSE),[12,13] as used for periodic compounds, is discussed in the present work by considering bulk silicon (Si), SiC, and LiF. The effect of the computational parameters controlling the calculation will be considered in the Si case for which high-quality experimental results[14−16] and many previous computations[17] are available. We will discuss, in particular, the influence of the percentage of "exact" exchange in the hybrid functionals on the UV-vis absorption spectrum (UV), electron loss function (ELF), and reflectivity (R), starting from the observation of Marques et al.[18] and the very recent work of Skone et al.[19] It is worth noting that, although the necessity of using hybrid functionals to compute reasonable band gaps has been frequently underlined recently, most of the applications compute the dynamic polarizability up to the first resonance only.[20−25] A systematic investigation of the effect of the "exact" exchange on the UV, ELF, and R functions of solids (from small gap semiconductors to insulators) is still lacking.

In the next section, entitled "Frequency-Dependent CPHF-(KS)", we first recall the frequency-dependent CPHF(KS) basic equations implemented in the CRYSTAL code and how the

Received: March 2, 2015

DOI: 10.1021/acs.jctc.5b00199
J. Chem. Theory Comput. XXXX, XXX, XXX−XXX

exciton effects can appear in the UV range. We then discuss the effect of the computational parameters in the case of Si. Moreover, in the last section, the UV spectra, as well as the ELF and R values, for a small-gap semiconductor (Si), a wide gap semiconductor (SiC), and an insulator (LiF) are compared.

FREQUENCY-DEPENDENT CPHF(KS)

The Optical Dielectric Constant. The Cartesian components of the static polarizability α_{uv}, and the related elements of the dielectric constant, are calculated as follows in the AO basis set (μ,ν):

$$\alpha_{uv} = -\frac{4}{n_k}\sum_{\mathbf{k}}^{\mathrm{BZ}} \mathcal{R}_e\left\{\sum_{\mu\nu}\sum_{i}^{\mathrm{occ}}\sum_{a}^{\mathrm{virt}} C^{\mathbf{k}*}_{\mu i}\Omega^{\mathbf{k},v}_{\mu\nu}C^{\mathbf{k}}_{\nu a}U^{u}_{ia,\mathbf{k}}\right\} \tag{1}$$

$$\epsilon^{\infty}_{uv} = \delta_{uv} + \left(\frac{4\pi}{V}\right)\alpha_{uv} \tag{2}$$

where n_k is the number of $\mathbf{k}$ points in the first Brillouin Zone (BZ) and the indices i (j) and a (b) span the occupied and virtual crystalline orbitals, respectively, and where V is the volume of the cell containing twice more electrons than occupied orbitals per k-point for closed-shell systems. $U^{u}_{\mathbf{k}}$ is the unknown anti-Hermitian off-diagonal-block matrix that linearly transforms the unperturbed eigenvectors $C^{\mathbf{k}}$ under the effect of the electric field perturbation represented by matrix $\Omega^{\mathbf{k}}$ (and later defined in the text):

$$\mathbb{C}^{\mathbf{k},u}_{\mu i} \equiv \left.\frac{\partial C^{\mathbf{k}}_{\mu i}}{\partial \varepsilon_u}\right|_0 = \sum_{l}^{\mathrm{all}} C^{\mathbf{k}}_{\mu l}U^{u}_{il,\mathbf{k}} \tag{3}$$

The off-diagonal (occupied-virtual) blocks $U^{u}_{ia,\mathbf{k}}$, defined as

$$U^{u}_{ia,\mathbf{k}} = \frac{\sum_{\mu\nu} C^{\mathbf{k}*}_{\mu a}\mathbb{F}^{\mathbf{k},u}_{\mu\nu}C^{\mathbf{k}}_{\nu i}}{\epsilon^{(0)}_{i_{\mathbf{k}}} - \epsilon^{(0)}_{a_{\mathbf{k}}}} \tag{4}$$

are functions of both the energy gap $(\epsilon^{(0)}_{i_{\mathbf{k}}} - \epsilon^{(0)}_{a_{\mathbf{k}}})$, and the perturbed Fock matrix (Hartree−Fock Hamiltonian),[2]

$$\begin{aligned}\mathbb{F}^{\mathbf{k},u}_{\mu\nu} &\equiv \left.\frac{\partial F^{\mathbf{k}}_{\mu\nu}}{\partial \varepsilon_u}\right|_0 \\ &= \Omega^{\mathbf{k},u}_{\mu\nu} + \sum_{\mathbf{g}} e^{\imath\mathbf{k}\cdot\mathbf{g}}\sum_{\lambda\rho}\sum_{\mathbf{k}'}^{BZ}\sum_{\mathbf{g}'} e^{-\imath\mathbf{k}'\cdot\mathbf{g}'}\sum_{j}(\mathbb{C}^{\mathbf{k}',u}_{\lambda j}C^{\mathbf{k}'*}_{\rho j} + C^{\mathbf{k}'}_{\lambda j}\mathbb{C}^{\mathbf{k}',*}_{\rho j}) \\ &\quad\times\sum_{\mathbf{g}''}[2(\mu^{\mathbf{0}}\nu^{\mathbf{g}}|\lambda^{\mathbf{g}''}\rho^{\mathbf{g}'+\mathbf{g}''}) - (\mu^{\mathbf{0}}\lambda^{\mathbf{g}''}|\nu^{\mathbf{g}}\rho^{\mathbf{g}'+\mathbf{g}''})]\end{aligned} \tag{5}$$

Moving from the Bloch (AO) basis to the crystalline orbitals (CO) basis, we obtain

$$\begin{aligned}\mathbb{F}^{u}_{ia,\mathbf{k}} &= \sum_{\mu\nu} C^{\mathbf{k}*}_{\mu a}\mathbb{F}^{\mathbf{k},u}_{\mu\nu}C^{\mathbf{k}}_{\nu i} \\ &= \Omega^{u}_{ia,\mathbf{k}} + \sum_{\mathbf{k}'}^{\mathrm{BZ}}\sum_{j}\sum_{b} U^{u}_{jb,\mathbf{k}}B^{jb,\mathbf{k}'}_{ia,\mathbf{k}} + U^{u*}_{jb,\mathbf{k}}B^{bj,\mathbf{k}'}_{ia,\mathbf{k}}\end{aligned} \tag{6}$$

where $\Omega^{u}_{ia,\mathbf{k}}$ is the transition moment operator for periodic systems[26] (defined as $\Omega^{u}_{ia,\mathbf{k}} = \langle i_{\mathbf{k}}|u + \imath(\mathrm{d}/\mathrm{d}\mathbf{k}_u)|a_{\mathbf{k}}\rangle$, where $u = x$, y, or z) between occupied $i_{\mathbf{k}}$ and virtual $a_{\mathbf{k}}$ crystalline orbitals with unperturbed eigenvalues $\epsilon^{(0)}_{i_{\mathbf{k}}}$ and $\epsilon^{(0)}_{a_{\mathbf{k}}}$, respectively, for each $\mathbf{k}$-point of the periodic system. This expression of the Ω-operator holds if the wave vector $\mathbf{q}$ of the field is close to zero[27] (i.e., the wavelength is much larger than the unit-cell size) condition that is valid for the static case and for the UV-vis light. The $B^{jb,\mathbf{k}'}_{ia,\mathbf{k}}$ and $B^{bj,\mathbf{k}'}_{ia,\mathbf{k}}$ terms are defined as follows:

$$B^{jb,\mathbf{k}'}_{ia,\mathbf{k}} = [2\langle i_{\mathbf{k}}b_{\mathbf{k}}|a_{\mathbf{k}}j_{\mathbf{k}'}\rangle - \langle i_{\mathbf{k}}b_{\mathbf{k}'}|j_{\mathbf{k}'}a_{\mathbf{k}}\rangle] \tag{7}$$

$$B^{bj,\mathbf{k}'}_{ia,\mathbf{k}} = [2\langle i_{\mathbf{k}}j_{\mathbf{k}'}|a_{\mathbf{k}}b_{\mathbf{k}'}\rangle - \langle i_{\mathbf{k}}j_{\mathbf{k}'}|b_{\mathbf{k}'}a_{\mathbf{k}}\rangle] \tag{8}$$

The notation $\langle ij|ab\rangle$ is used for the bielectronic integral $\langle i(1)j(2)|(1/r_{12})|a(1)b(2)\rangle$.

Then, $U^{u}_{\mathbf{k}}$ (eq 4) for a given $\mathbf{k}$-point is dependent on $\mathbb{F}^{u}_{\mathbf{k}}$ (eq 6), which, in turn, is dependent on the $U^{u}_{\mathbf{k}'}$ matrices for all $\mathbf{k}$-points. Hence, a self-consistent coupled-perturbed (SC-CP) process is to be carried out (CPHF or CPKS). At the first cycle of the process, the derivative of the density matrix, with respect to the field, is equal to zero and there is no bielectronic contribution in $\mathbb{F}^{u}_{ia,\mathbf{k}}$. This step of unrelaxed orbitals corresponds to the Sum Over States approximation (SOS).

If the field is frequency(ω)-dependent, the time-dependent perturbation theory leads to the two following $U^{\pm}$ matrices (see refs 9 and 28 for the molecular or $\mathbf{k} = \mathbf{0}$ cases, and ref 6 for periodic systems):

$$U^{u\pm[n]}_{ia,\mathbf{k}} = \lim_{\eta\to 0^+}\frac{\Omega^{u}_{ia,\mathbf{k}} + \sum_{\mathbf{k}'}\sum_{j}^{\mathrm{occ}}\sum_{b}^{\mathrm{virt}}(U^{u\pm[n-1]}_{jb,\mathbf{k}'}B^{jb,\mathbf{k}'}_{ia,\mathbf{k}} + U^{u\mp*[n-1]}_{jb,\mathbf{k}'}B^{bj,\mathbf{k}'}_{ia,\mathbf{k}})}{\epsilon^{(0)}_{i_{\mathbf{k}}} - \epsilon^{(0)}_{a_{\mathbf{k}}} \pm \omega + \imath\eta} \tag{9}$$

where η is a damping factor that produces peak broadening when the inverse of the lifetime of excited states is taken into account. This is not easily evaluated in solids and, usually, the energy resolution of the experimental equipment is used instead ($\eta \simeq 0.1$ eV in the UV-vis range). The equivalent of eq 2 in the frequency-dependent case is

$$\begin{aligned}\mathcal{R}e(\epsilon^{\infty}_{uv}(\omega)) &= \delta_{uv} + \left(\frac{4\pi}{V}\right)\alpha_{uv}(\omega) \\ &= \delta_{uv} - \frac{8\pi}{V}\left(\frac{1}{n_k}\right)\mathcal{R}_e\sum_{\mathbf{k}}^{\mathrm{BZ}}\sum_{i}^{\mathrm{occ}}\sum_{a}^{\mathrm{virt}}\Omega^{v}_{ai,\mathbf{k}}(U^{u+}_{ia,\mathbf{k}} + U^{u-}_{ia,\mathbf{k}})\end{aligned} \tag{10}$$

Note that the dielectric matrix elements are real if $\eta = 0$: $\epsilon^{\infty}_{uv}(\omega) = \mathcal{R}e(\epsilon^{\infty}_{uv}(\omega))$.

To better understand the origin of the energy of the pole, let us separate the "diagonal" $(i = j, a = b, \mathbf{k} = \mathbf{k}')$ bielectronic term from all others in eq 9 at the convergence of the iterative SC-CP process (where $U^{u\pm[n]}_{ia,\mathbf{k}} \simeq U^{u\pm[n-1]}_{ia,\mathbf{k}} \simeq U^{u\pm}_{ia,\mathbf{k}}$):

$$U^{u\pm}_{ia,\mathbf{k}} = \frac{\Omega^{u}_{ia,\mathbf{k}} + U^{u\pm}_{ia,\mathbf{k}}B^{ia,\mathbf{k}}_{ia,\mathbf{k}} + U^{u\mp*}_{ia,\mathbf{k}}B^{ai,\mathbf{k}}_{ia,\mathbf{k}} + \sum_{(\mathbf{k}',j,b)\neq(\mathbf{k},i,a)}(U^{u\pm}_{jb,\mathbf{k}}B^{jb,\mathbf{k}'}_{ia,\mathbf{k}} + U^{u\mp*}_{jb,\mathbf{k}'}B^{bj,\mathbf{k}'}_{ia,\mathbf{k}})}{\epsilon^{(0)}_{i_{\mathbf{k}}} - \epsilon^{(0)}_{a_{\mathbf{k}}} \pm \omega + \imath\eta} \tag{11}$$

This matrix element can be written as follows:

$$U^{u\pm}_{ia,\mathbf{k}} = \frac{\Omega^{u}_{ia,\mathbf{k}} + U^{u\mp*}_{ia,\mathbf{k}}B^{ai,\mathbf{k}}_{ia,\mathbf{k}} + \sum_{(\mathbf{k}',j,b)\neq(\mathbf{k},i,a)}(U^{u\pm}_{jb,\mathbf{k}}B^{jb,\mathbf{k}'}_{ia,\mathbf{k}} + U^{u\mp*}_{jb,\mathbf{k}}B^{bj,\mathbf{k}'}_{ia,\mathbf{k}})}{\epsilon^{(0)}_{i_{\mathbf{k}}} - \epsilon^{(0)}_{a_{\mathbf{k}}} - B^{ia,\mathbf{k}}_{ia,\mathbf{k}} \pm \omega + \imath\eta} \tag{12}$$

[In going from eq 11 to eq 12, we use $x = (a + bx)/c \Rightarrow x(1 - b/c) = a/c$, which leads to $x = a/(c - b)$.]

Resonance. Before looking at the expression of $\mathcal{I}m(\epsilon^{\infty}_{uv}(\omega))$, which provides the UV spectrum, we want to

DOI: 10.1021/acs.jctc.5b00199
J. Chem. Theory Comput. XXXX, XXX, XXX−XXX

underline the relevance of eq 12. Although eqs 11 and 12 are formally equivalent, eq 12 makes the SC-CP procedure much clearer. In the SOS approximation for real $U^{u+}_{ia,\mathbf{k}}$ ($\eta \to 0$):

$$U^{u+}_{ia,\mathbf{k}} = \frac{\Omega^{u}_{ia,\mathbf{k}}}{\epsilon^{(0)}_{i_\mathbf{k}} - \epsilon^{(0)}_{a_\mathbf{k}} + \omega} \tag{13}$$

the resonance occurs at $\omega = \epsilon^{(0)}_{a_\mathbf{k}} - \epsilon^{(0)}_{i_\mathbf{k}}$. However, eq 12 shows that, when the system responds to the perturbation (the SC-CP scheme is active), the resonance is shifted by $B^{ia,\mathbf{k}}_{ia,\mathbf{k}}$. The $U^{u+}_{ia,\mathbf{k}}$ element becomes infinite near the new resonance ω (which is defined as $\omega = \omega_{ia,\mathbf{k}} = \epsilon^{(0)}_{a_\mathbf{k}} - \epsilon^{(0)}_{i_\mathbf{k}} + B^{ia,\mathbf{k}}_{ia,\mathbf{k}}$), where the denominator tends to zero. We can do the further step by considering now the behavior of $U^{u-}_{ia,\mathbf{k}}$ in eq 12. At resonance, the denominator is not null (due to a negative sign of ω), but the numerator tends to infinity because of the presence of $U^{u+}_{ia,\mathbf{k}}$. So we have $U^{u-}_{ia,\mathbf{k}} \simeq U^{u+*}_{ia,\mathbf{k}} B^{ai,\mathbf{k}}_{ia,\mathbf{k}} / (\epsilon^{(0)}_{i_\mathbf{k}} - \epsilon^{(0)}_{a_\mathbf{k}} - B^{ia,\mathbf{k}}_{ia,\mathbf{k}} - \omega_{ia,\mathbf{k}})$. The $U^{u-*}_{ia,\mathbf{k}}$ element, which appears in the numerator of eq 12 for $U^{u+}_{ia,\mathbf{k}}$, is equal to $-U^{u+}_{ia,\mathbf{k}} B^{ai,\mathbf{k}}_{ia,\mathbf{k}} / (2\omega_{ia,\mathbf{k}})$. The expression of $U^{u+}_{ia,\mathbf{k}}$ in eq 12 then becomes

$$U^{u+}_{ia,\mathbf{k}} \simeq \frac{\Omega^{u}_{ia,\mathbf{k}}}{\epsilon^{(0)}_{i_\mathbf{k}} - \epsilon^{(0)}_{a_\mathbf{k}} - B^{ia,\mathbf{k}}_{ia,\mathbf{k}} + (B^{ai,\mathbf{k}}_{ia,\mathbf{k}})^2 / 2\omega_{ia,\mathbf{k}} + \omega} \tag{14}$$

[Again, in going from eq 11 to eq 12, we use $x = (a + bx)/c \Rightarrow x(1 - b/c) = a/c$, which leads to $x = a/(c-b)$.] This means that the pole is shifted, with respect to SOS, by $B^{ia,\mathbf{k}}_{ia,\mathbf{k}} = 2\langle i_\mathbf{k} a_\mathbf{k} |\, a_\mathbf{k} i_\mathbf{k}\rangle - \langle i_\mathbf{k} a_\mathbf{k} | i_\mathbf{k} a_\mathbf{k}\rangle$ (first-order correction), and by something depending on $B^{ai,\mathbf{k}}_{ia,\mathbf{k}} = \langle i_\mathbf{k} i_\mathbf{k} |\, a_\mathbf{k} a_\mathbf{k}\rangle$ (see eqs 7 and 8; note also the interchange between ia and ai).

In solids, where the density of states (in the valence and conduction bands) is a continuous function of the energy, the summation on $\mathbf{k}'$, b, and j cannot be disregarded because several other transitions $j_{\mathbf{k}'} \to b_{\mathbf{k}'}$ may occur around $\omega_{ia,\mathbf{k}}$ for which we can assume that $U^{u+}_{jb,\mathbf{k}'} / U^{u+}_{ia,\mathbf{k}} \simeq \Omega^{u}_{jb,\mathbf{k}'} / \Omega^{u}_{ia,\mathbf{k}}$ (in eq 14, the denominator for $U^{u+}_{ia,\mathbf{k}}$ and $U^{u+}_{jb,\mathbf{k}'}$ is roughly the same). The resulting bielectronic terms $U^{u+}_{jb,\mathbf{k}'} B^{jb,\mathbf{k}'}_{ia,\mathbf{k}}$ in the numerator of $U^{u+}_{ia,\mathbf{k}}$ (eq 12) can be moved outside the summation once weighted by the density $\rho(\omega_{ia,\mathbf{k}})$, representing the number of transitions $j_{\mathbf{k}'} \to b_{\mathbf{k}'}$ for which the transition energy $\omega_{jb,\mathbf{k}'}$ is close to $\omega_{ia,\mathbf{k}}$. Then, at resonance, eq 11 (for $\eta = 0$) can be replaced by

$$U^{u+}_{ia,\mathbf{k}} = \frac{\bar{\Omega}^{u}_{ia,\mathbf{k}}}{\epsilon^{(0)}_{i_\mathbf{k}} - \epsilon^{(0)}_{a_\mathbf{k}} - \rho(\omega_{ia,\mathbf{k}}) \bar{B}^{jb,\mathbf{k}'}_{ia,\mathbf{k}} + \omega} \tag{15}$$

In the above equation, $\bar{B}^{jb,\mathbf{k}'}_{ia,\mathbf{k}}$ includes all the contributions from the bielectronic integral between orbitals involved in transitions with an energy value close to the pole:

$$\omega_{ia,\mathbf{k}} = \epsilon^{(0)}_{a_\mathbf{k}} - \epsilon^{(0)}_{i_\mathbf{k}} + \rho(\omega_{ia,\mathbf{k}}) \bar{B}^{jb,\mathbf{k}'}_{ia,\mathbf{k}} \tag{16}$$

and $\overline{\Omega}^{u}_{ia,\mathbf{k}}$ is equal to $\Omega^{u}_{ia,\mathbf{k}}$ corrected by all the other bielectronic $B^{j'b',\mathbf{k}'}_{ia,\mathbf{k}}$ and $B^{b'j',\mathbf{k}'}_{ia,\mathbf{k}}$ contributions corresponding to transitions $j_{\mathbf{k}'} \to b_{\mathbf{k}'}$ far in energy from $\omega_{ia,\mathbf{k}}$.

Imaginary Part of the Dielectric Constant. When $\eta \neq 0$, near resonance, the imaginary part of the complex dielectric constant can be written as follows (see eqs 10 and 15):

$$\mathcal{I}_m(\epsilon^{\infty}_{uv}(\omega)) = \frac{8\pi}{V n_k} \sum_{\mathbf{k}}^{\mathrm{BZ}} \sum_{i}^{\mathrm{occ}} \sum_{a}^{\mathrm{virt}} \frac{\eta \mathcal{R}_e(\Omega^{v*}_{ia,\mathbf{k}} \bar{\Omega}^{u}_{ia,\mathbf{k}})}{(\omega_{ia,\mathbf{k}} - \omega)^2 + \eta^2} \tag{17}$$

The nonresonant $U^{u-}_{ia,\mathbf{k}}$ terms have been neglected in the previous equation, since they are expected to give negligible contributions to the resonance. Actually they can be calculated directly without any approximation from the product of $\Omega^{u}_{ia,\mathbf{k}}$ and $U^{u-}_{ia,\mathbf{k}}$ in eq 11.

The case of the resonant $U^{u+}_{ia,\mathbf{k}}$ term is more delicate. Expression 11 seems to show that the damping factor becomes important when $\omega_{ia,\mathbf{k}} = \epsilon^{(0)}_{a_\mathbf{k}} - \epsilon^{(0)}_{i_\mathbf{k}}$; eq 12, however, shows that a shift by $\rho(\omega_{ia,\mathbf{k}}) \bar{B}^{jb,\mathbf{k}'}_{ia,\mathbf{k}}$ must be taken into account. If, then, eq 11 is used as such in the calculation, it turns out that the imaginary part of $U^{u+}_{ia,\mathbf{k}}$ is changing sign in the $[\epsilon^{(0)}_{a_\mathbf{k}} - \epsilon^{(0)}_{i_\mathbf{k}} + \rho(\omega_{ia,\mathbf{k}}) \bar{B}^{jb,\mathbf{k}'}_{ia,\mathbf{k}},\ \epsilon^{(0)}_{a_\mathbf{k}} - \epsilon^{(0)}_{i_\mathbf{k}}]$ interval (remember that $\mathcal{I}_m(\epsilon^{\infty}_{uv}(\omega))$ must be a positive quantity). An alternative equivalent formulation allows one to avoid large positive to negative oscillations around the resonance. From eq 15, we have

$$|\omega_{ia,\mathbf{k}} - \omega| = \left| \frac{\bar{\Omega}^{u}_{ia,\mathbf{k}}}{U^{u+}_{ia,\mathbf{k}}(\eta = 0)} \right| \tag{18}$$

The denominator in eq 17 can be recast as

$$\begin{aligned} \mathcal{I}_m(\epsilon^{\infty}_{uv}(\omega)) &= \frac{8\pi}{V n_k} \sum_{\mathbf{k}}^{\mathrm{BZ}} \sum_{i}^{\mathrm{occ}} \sum_{a}^{\mathrm{virt}} \frac{\eta \mathcal{R}_e(\Omega^{v*}_{ia,\mathbf{k}} \bar{\Omega}^{u}_{ia,\mathbf{k}})}{|\bar{\Omega}^{u}_{ia,\mathbf{k}} / U^{u+}_{ia,\mathbf{k}}(\eta = 0)|^2 + \eta^2} \\ &= \frac{8\pi}{V n_k} \sum_{\mathbf{k}}^{\mathrm{BZ}} \sum_{i}^{\mathrm{occ}} \sum_{a}^{\mathrm{virt}} \frac{\eta \mathcal{R}_e(\Omega^{v*}_{ia,\mathbf{k}} \bar{\Omega}^{u}_{ia,\mathbf{k}})}{\bar{\Omega}^{u*}_{ia,\mathbf{k}} \bar{\Omega}^{u}_{ia,\mathbf{k}}} |U^{u+}_{ia,\mathbf{k}}|^2 \end{aligned} \tag{19}$$

where, in the second step, we used the square modulus of eq 15 (but with $\eta \neq 0$). The above function is proportional to η and, then, close to zero, when far from resonance ($|\bar{\Omega}^{u}_{ia,\mathbf{k}} / U^{u+}_{ia,\mathbf{k}}| \gg \eta$); near the resonance, it is inversely proportional to η and large. In that case, the imaginary part of the dielectric constant is proportional to the product of the transition moments $\Omega^{u*}_{ia,\mathbf{k}} \bar{\Omega}^{u}_{ia,\mathbf{k}}$ multiplied by the new density of transitions $\rho(\omega_{ia,\mathbf{k}})$ (as the $i_\mathbf{k}$ and $a_\mathbf{k}$ functions extend to all the cases such as $\omega_{ia,\mathbf{k}} = \epsilon^{(0)}_{a_\mathbf{k}} - \epsilon^{(0)}_{i_\mathbf{k}} + \rho(\omega_{ia,\mathbf{k}}) \bar{B}^{jb,\mathbf{k}'}_{ia,\mathbf{k}}$). Until now, no approximation has been introduced in the expression of the imaginary part of the dielectric constant, but the presence of $\bar{\Omega}_{ia,\mathbf{k}}$ shows that we need to calculate the correction on the transition moment $\Omega^{u}_{ia,\mathbf{k}}$ due to bielectronic integral contributions ($U^{u\pm}_{jb,\mathbf{k}} B^{jb,\mathbf{k}'}_{ia,\mathbf{k}}$ and $U^{u\pm}_{jb,\mathbf{k}'} B^{bj,\mathbf{k}'}_{ia,\mathbf{k}}$) involving nonresonant $j_{\mathbf{k}'} \to b_{\mathbf{k}'}$ transitions (see eq 12). This correction should be small if these nonresonant transitions are far from the present $i_\mathbf{k} \to a_\mathbf{k}$ resonant transition and not too numerous (the case of molecules but probably not of periodic systems). Nevertheless, they have been neglected in the imaginary part of the dielectric constant of which the expression (diagonal component) finally becomes

$$\mathcal{I}_m(\epsilon^{\infty}_{uu}(\omega)) \simeq \frac{8\pi}{V n_k} \sum_{\mathbf{k}}^{\mathrm{BZ}} \sum_{i}^{\mathrm{occ}} \sum_{a}^{\mathrm{virt}} \eta |U^{u+}_{ia,\mathbf{k}}|^2 \tag{20}$$

when replacing $\bar{\Omega}^{u}_{ia,\mathbf{k}}$ with $\Omega^{u}_{ia,\mathbf{k}}$ in eq 19.

However, a decrease in the numerator of $\mathcal{I}_m(\epsilon^{\infty}_{uu}(\omega))$ due to coupling corrections in eq 19 on the transition moment should lead to a decrease in the peak height and an increase in its full width at half-maximum (fwhm), and vice versa, with no drastic change in the integral of the spectrum.

Oscillator Strength. The multiplication of the imaginary part of the dielectric constant (eq 20) by $2\omega/(4\pi/V)$ leads to the oscillator strength at each frequency ω (i.e., to the UV spectrum). The integration of the spectrum over ω leads to

DOI: 10.1021/acs.jctc.5b00199
J. Chem. Theory Comput. XXXX, XXX, XXX−XXX

$$\frac{1}{\pi}\int_0^\infty \frac{2\omega \mathcal{I}_m(\epsilon^\infty_{uu}(\omega))}{(4\pi/V)}\,\mathrm{d}\omega = \frac{2}{n_k}\sum_{\mathbf{k}}^{\mathrm{BZ}}\sum_i^{\mathrm{occ}}\sum_a^{\mathrm{virt}}\frac{1}{\pi}\int_0^\infty \frac{2\omega\eta|\Omega^u_{ai,\mathbf{k}}|^2}{(\omega_{ia,\mathbf{k}}-\omega)^2+\eta^2}\,\mathrm{d}\omega = \frac{2}{n_k}\sum_{\mathbf{k}}^{\mathrm{BZ}}\sum_i^{\mathrm{occ}}\sum_a^{\mathrm{virt}} 2\omega_{ia,\mathbf{k}}|\Omega^u_{ai,\mathbf{k}}|^2 \quad (21)$$

with each transition intensity being a Lorentzian function with height $1/\eta$ and width 2η for which the integration is π. In the case of pure DFT, orbitals are obeying the hypervirial relation (for a large enough AO basis set[27]):

$$(\epsilon^{(0)}_{i_\mathbf{k}} - \epsilon^{(0)}_{a_\mathbf{k}})\Omega^u_{ia,\mathbf{k}} = -\nabla^u_{ia,\mathbf{k}} \quad (22)$$

where $\nabla^u = \mathrm{d}/\mathrm{d}u$ acts in the direct space.

The sum over oscillator strengths obtained in eq 21 then is equal to the number of valence electrons involved in the UV range (the Thomas−Reiche−Kuhn sum rule),

$$\frac{2}{n_k}\sum_{\mathbf{k}}^{\mathrm{BZ}}\sum_i^{\mathrm{occ}}\sum_a^{\mathrm{virt}} 2(\epsilon^{(0)}_{a_\mathbf{k}} - \epsilon^{(0)}_{i_\mathbf{k}})|\Omega^u_{ia,\mathbf{k}}|^2 = \frac{2}{n_k}\sum_{\mathbf{k}}^{\mathrm{BZ}}\sum_i^{\mathrm{occ}}\sum_a^{\mathrm{virt}} 2\nabla^u_{ia,\mathbf{k}}\Omega^u_{ai,\mathbf{k}} = \frac{2}{n_k}\sum_{\mathbf{k}}^{\mathrm{BZ}}\sum_i^{\mathrm{occ}} 2\langle i_\mathbf{k}|\nabla^u\Omega^u|i_\mathbf{k}\rangle = n_e \quad (23)$$

if the basis set is complete. The number of electrons n_e on the right-hand side of the above equation is obtained considering that $-\imath\nabla^u = -\imath\mathrm{d}/\mathrm{d}u$ and $\Omega^u = u + \imath\mathrm{d}/\mathrm{d}k_u$ $(= \imath e^{i\mathbf{k}\cdot\mathbf{r}}\nabla_{k_u}e^{-i\mathbf{k}\cdot\mathbf{r}})$ are Hermitian operators. With hybrid Hamiltonians, the UV surface is not equal to the number of electrons, since eq 22 is not valid, because of the noncommutativity of $\mathbf{r}$-position and HF-exchange (non local) operators, and also because $\overline{\Omega}^u_{ia,\mathbf{k}}$ has been replaced by $\Omega^u_{ia,\mathbf{k}}$ in eq 19. It follows an amplification of the peak intensities (with respect to SOS ones obtained with the same η value), which can be renormalized *a posteriori* by the value of the full UV integration.

COMPUTATIONAL DETAILS

Calculations were performed with a development version of the periodic *ab initio* CRYSTAL14 code. Several functionals have been tested: the local LDA,[29,30] the gradient-corrected PBE[31] and the hybrid B3LYP.[32,33]

In addition, the dependence of the dielectric function on the amount of exact exchange incorporated into the hybrid functional has been tested by considering a different percentage (x) of exact exchange, with respect to the standard value (25% in B3LYP): x = 10% (F10LYP), x = 15% (F15LYP), x = 40% (F40LYP), and x = 50% (F50LYP).

The following basis sets have been used (see refs 27 and 34): 8-8411-11 [1s4sp2d] (Si), 6-21-11 [1s2sp2d] (C), 7-311-1 [1s2sp1d] (F), and a 6-1-1 [1s1sp1p] (Li).

In the CRYSTAL code, the level of accuracy in evaluating the Coulomb and exchange integrals is controlled by five T parameters ($T1 = T2 = T3$, $T4$, $T5 = 2T4$) (see ref 3). The first two parameters control the Coulomb series and the latter three control the exchange series. Several selections of $T = (T1,T4)$ have been tested in the present calculations, ranging from T = (8,8) to T = (10,25) (used as a reference).

The k-grid mesh is controlled in the CRYSTAL code by the shrinking factor IS. Increasing values of IS have been considered: 16, 36 and 100, corresponding to 145, 1240, and 22000 k-points, respectively, for a cubic lattice.

A damping factor η (eq 9) selected in the range of 0.03−0.1 eV has been found to provide stable results (a value of η = 0.055 eV is used if not otherwise specified).

The difficulty to obtain the limit of $U^{u+}_{ia,\mathbf{k}}$ iteratively appears when $\omega = \epsilon^{(0)}_{a_\mathbf{k}} - \epsilon^{(0)}_{i_\mathbf{k}}$, i.e. when the numerator and denominator in eq 9 are both equal to zero (if η is null), while this limit is well-defined and equal to $-\Omega^u_{ia,\mathbf{k}}/(\rho(\omega_{ia,\mathbf{k}})\ \overline{B}^{\ jb,\mathbf{k}'}_{ia,\mathbf{k}})$ near this transition energy (use eq 15 with $\omega = \epsilon^{(0)}_{a_\mathbf{k}} - \epsilon^{(0)}_{i_\mathbf{k}}$). Actually, the SC-CP process is similar to the numerical Gauss−Seidel method[35] for solving large linear equations systems: $AX = B$, where X represents the unknown vector (the U-vector in the present work), B the dynamic field perturbation, and A the projected time-dependent Hamiltonian $H - \imath\hbar\,\mathrm{d}/\mathrm{d}t$ in the single occupied-virtual excitation basis set. The Gauss−Seidel method is particularly efficient when the matrix A is diagonal dominant. However, if one or more diagonal terms of the A matrix is close to zero, the solution does not converge any more. This happens near resonances and a mathematical algorithm is required to force the convergence of the iterative process. The epsilon-algorithm-2[36,37] using the X-vector obtained from the previous 2-iterations has been used after each four SC-CP iterations in the entire range of the UV-vis absorption energy, and convergence has been reached for most of the field frequencies. The SC-CP process then is prevented because of the storage of a huge Hamiltonian matrix (with off-diagonal $B^{jb,\mathbf{k}'}_{ia,\mathbf{k}}$ elements) before its diagonalization.

In order to facilitate comparison between UV spectra, the imaginary part of the dielectric constant is first broadened with Lorentzian functions. Then, the integration of $2\omega\mathcal{I}_m(\epsilon(\omega))$ over ω (which theoretically leads to the number of valence electrons involved in the spectrum; see eqs 21−23) then allows one to renormalize each plot of $\mathcal{I}_m(\epsilon)$ *a posteriori*.

APPLICATIONS

Silicon. *Electron Structure.* The band structure (BS) and projected density of states (PDOS) of silicon are reported in Figure S1 in the Supporting Information (ESI). Details of the BS close to the Fermi level E_F have been sketched, considering several special points in the reciprocal space, namely, Γ = (0 0 0), X = (0, $^1/_2$, $^1/_2$), W = ($^1/_4$, $^3/_4$, $^1/_2$), U = ($^1/_4$, $^5/_8$, $^5/_8$) and K = ($^3/_8$, $^3/_4$, $^3/_8$). Here, we summarize the main features. The valence bands (VBs) (bands from 11 to 14) and the conduction bands (CBs) are largely due to 3sp orbitals. VBs cover a range of ∼13 eV and CB extends for more than 25 eV (B3LYP, see Figure S1 and Table S1 in the ESI). The 2sp orbitals contribute to core states (∼100 eV below E_F) and to virtual states (50−100 eV above E_F). The highest occupied VB and the lowest unoccupied CB will be referenced hereafter referred as HOMO and LUMO, for analogy with the molecular case. Si has an indirect gap $E_g(\Gamma\rightarrow W)$ = 2.02 eV and a direct band gap in Γ, $E_g(\Gamma)$ = 3.77 eV; at L, $E_g(L)$ is equal to 3.96 eV and, then, quite close to $E_g(\Gamma)$. At the other special $\mathbf{k}$ points, the gap is much larger: $E_g(X)$ = 5.07 eV and $E_g(U(X))$ = 5.10 eV; the $E_{\mathrm{HOMO}\rightarrow\mathrm{LUMO+1}}(L)$ = 6.18 eV is the other lowest energy difference between the VB and CB bands (B3LYP results; see Table S1 in the ESI). PBE results are qualitatively similar to B3LYP, but energy differences are much smaller (by ∼1.5 eV). Intermediate values are provided by F10LYP and F15LYP functionals: for instance, F15LYP provides $E_g(\Gamma)$ = 3.52 eV, $E_g(X)$ = 5.07 eV, $E_g(U(X))$ = 5.10 eV and $E_{\mathrm{HOMO}\rightarrow\mathrm{LUMO+1}}(L)$ = 5.86 eV (see Table S1 in the ESI).

DOI: 10.1021/acs.jctc.5b00199
J. Chem. Theory Comput. XXXX, XXX, XXX−XXX

UV Spectrum. In this section, we discuss the computed UV spectrum and the influence of the computational parameters.

• Sampling the reciprocal space. $\mathcal{I}_m(e^{\infty})$-CP computed with the F10LYP functional and with several choices of IS (16, 36, and 100), is reported in Figure 1. With IS = 16, the computed spectrum is significantly different, with respect to the reference value (IS = 100), because of the presence of spurious peaks, that disappear by moving to IS = 36: in this case, both positions and heights of all the peaks are correctly predicted.

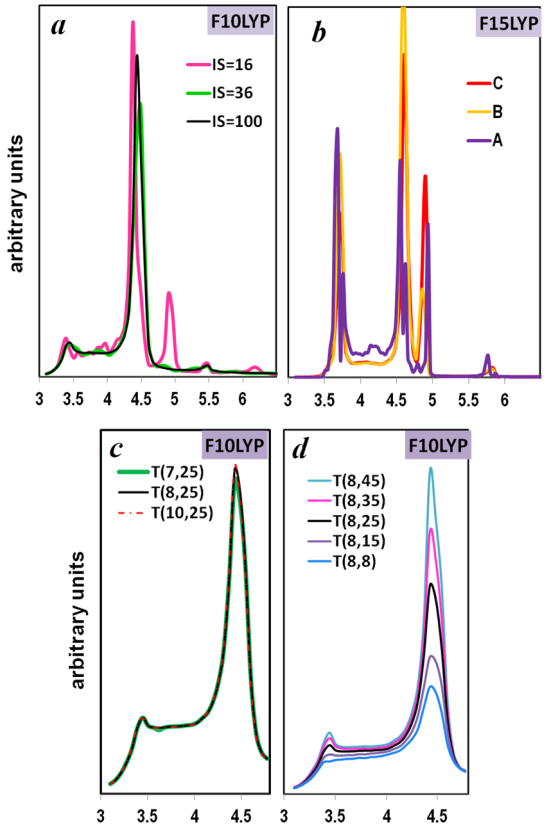

Figure 1. Effect of computational parameters on the imaginary part of the dielectric constant of silicon (SC-CP calculation): (a) reciprocal space sampling, IS, (T = (10,25) and η = 0.055 eV); (b) damping factor η: η = 0.055 eV (A), 0.082 eV (B), 0.11 eV (C), (T = 10,25 and IS = 100); (c, d) tolerances controlling the Coulomb and exchange series, T, (IS = 100 and η = 0.055 eV).

• Truncation of the Coulomb and exchange series. Figure 1 reports $\mathcal{I}_m(e^{\infty})$ (CP-F10LYP), as a function of the integral tolerance parameters T. The effect of the Coulomb series is a minor one, as shown by comparing T = (7,25) and T = (10,25). When the exchange integrals are involved in going from T = (8,8) to T = (8,45), the main effect is an enhancement of the intensity of the two main peaks, and more generally of the surface of the entire UV spectrum as it is explained in the subsection entitled "Oscillator Strength". However, the same ratio (0.20 ± 0.01) between the main peaks is roughly preserved when T increases.

• The damping factor η. The combination of η and number of points used to sample the energy range determines the resolution of the UV spectrum. In Figure 1, $\mathcal{I}_m(e)$-CP is reported for several values of η, namely, η = 0.055, 0.082, and 0.11 eV. For F10LYP, no significant change of the spectrum was found, while the F15LYP spectrum acquires more detail when η is smaller: each peak can be decomposed to one or more components. However, the position of the main peaks, and their relative intensity, are again not affected by this choice.

• The DFT functionals. $\mathcal{I}_m(e^{\infty})$-SOS and $\mathcal{I}_m(e^{\infty})$-CP spectra, computed with different functionals (LDA, PBE, F10LYP, F15LYP, and B3LYP) have been reported in Figure 2. The $\mathcal{I}_m(e^{\infty})$-SOS spectra show almost the same shape for all functionals. With respect to B3LYP, LDA and PBE are rigidly shifted to lower energies and F10LYP (F15LYP) is shifted to intermediate ones: the $\mathcal{I}_m(e^{\infty})$-SOS spectrum resembles the band structure as provided by the selected functional, and it is described by the vertical unperturbed $i_k \rightarrow a_k$ monoexcitations, the transition moment of which is $\Omega^{u}_{ia,k}$. Considering now the SC-CP calculation of $\mathcal{I}_m(e^{\infty})$, we see that, when pure DFT functionals are employed, the UV spectrum does not show any significant differences, with respect to the SOS counterpart (see Figure 2). The $\mathcal{I}_m(e^{\infty})$-CP spectrum of hybrid functionals, in contrast, takes a new shape, because of the presence of new peaks and enhancement of the previous SOS intensities, which is particularly evident in the 3.4−5.0 eV region.

F15LYP $\mathcal{I}_m(e^{\infty})$-CP computed with increasing resolutions are reported in Figures 1 and 2. The highly resolved spectrum (IS = 36, damping factor η = 0.5 mHa) shows several peaks: a

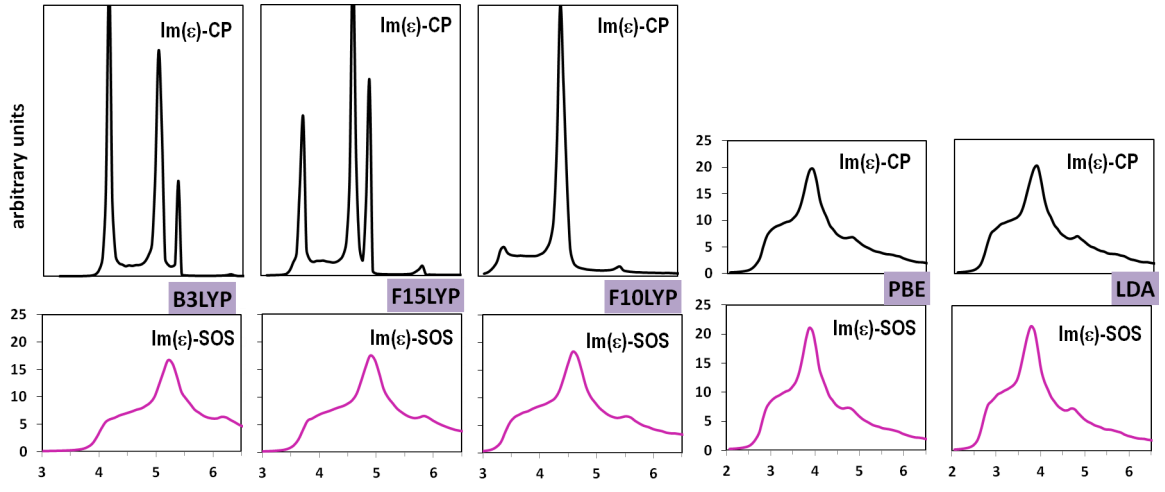

Figure 2. UV spectrum of silicon computed with different functionals. IS = 100, T = (10,25) and η = 0.055 eV.

DOI: 10.1021/acs.jctc.5b00199
J. Chem. Theory Comput. XXXX, XXX, XXX−XXX

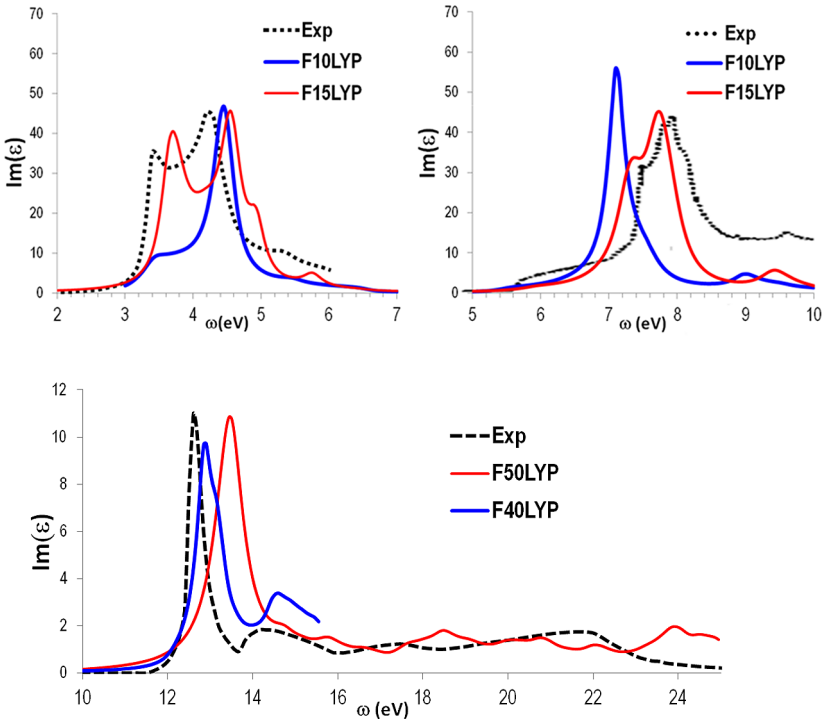

Figure 3. Computed and observed UV spectra of Si, SiC, and LiF. $\mathcal{I}_m(\epsilon)$-CP is obtained by normalizing and broadening the calculated spectrum with a Lorenztian function. Experimental spectra have been taken from refs 14, 41, and 45.

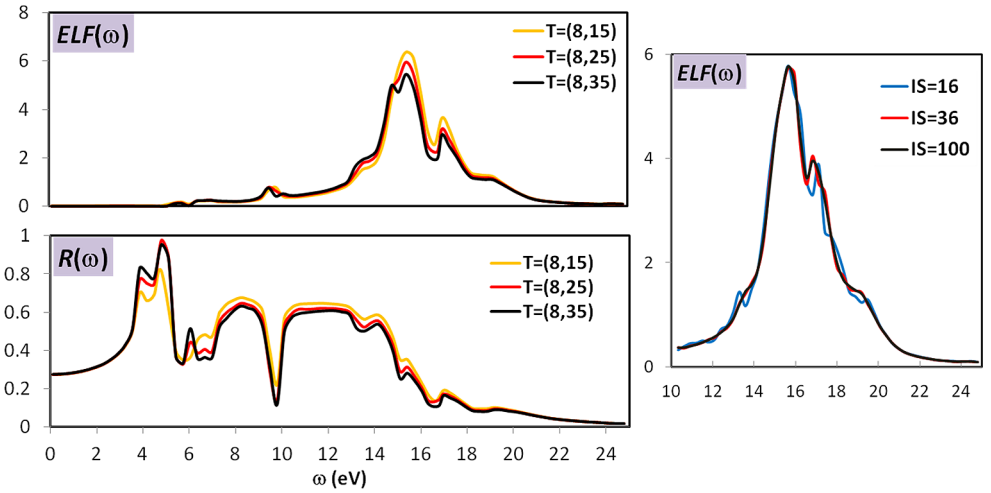

Figure 4. ELF(ω) and $R(\omega)$ of silicon at the SC-CP B3LYP level of calculation: effect of IS (T = 10,25 and η = 0.11 eV) (right panel) and T (IS = 100 and η = 0.11 eV) (left panels).

high-intensity doublet at 3.69 and 3.75 eV, another intense doublet at 4.55 and 4.62 eV, a peak at 4.93 eV, and a low-intensity one at 5.76 eV.

Comparison of the positions of each peak with the silicon BS (see Figure S1 and Table S1 in the ESI) allows the following assignments. The peaks in the first intense doublet are assigned to HOMO → LUMO transitions from oscillators in a narrow region around Γ (the former), and to L (the latter), whereas those in the second doublet are derived from HOMO → LUMO transitions in a large region around X; the 5.76 peak corresponds to HOMO → LUMO+1 transitions in a narrow region close to L. In ref 16, a detailed analysis of the experimental spectrum is reported. The spectrum is composed of several doublets: at 3.40 and 3.45 eV, at 4.18 and 4.22 eV, and at 4.44 and 4.60 eV, and a peak at 5.4 eV. Computed peaks are then in very good agreement with the observed ones, despite a slight shift (0.3−0.4 eV) toward higher energies. The F10LYP spectrum (see Figure 2) shows poles at 3.45, 4.49, and 5.48 eV. Although their positions are closer to the experimental ones, the intensity of the first peak is too low, compared to those at higher energy. The surface of the spectrum (in a polarized direction) has been found to be larger than the number of valence electrons (by 10% with SOS), and in order to make the comparison with the experimental spectra easier (see refs 14 and 16), the computed CPHF(KS) spectrum has been normalized *a posteriori* to match eq 23 (see Figure 3). The shape of the F15LYP spectrum, even if slightly shifted to higher energies, reproduces the observed one quite nicely, confirming

DOI: 10.1021/acs.jctc.5b00199
J. Chem. Theory Comput. XXXX, XXX, XXX−XXX

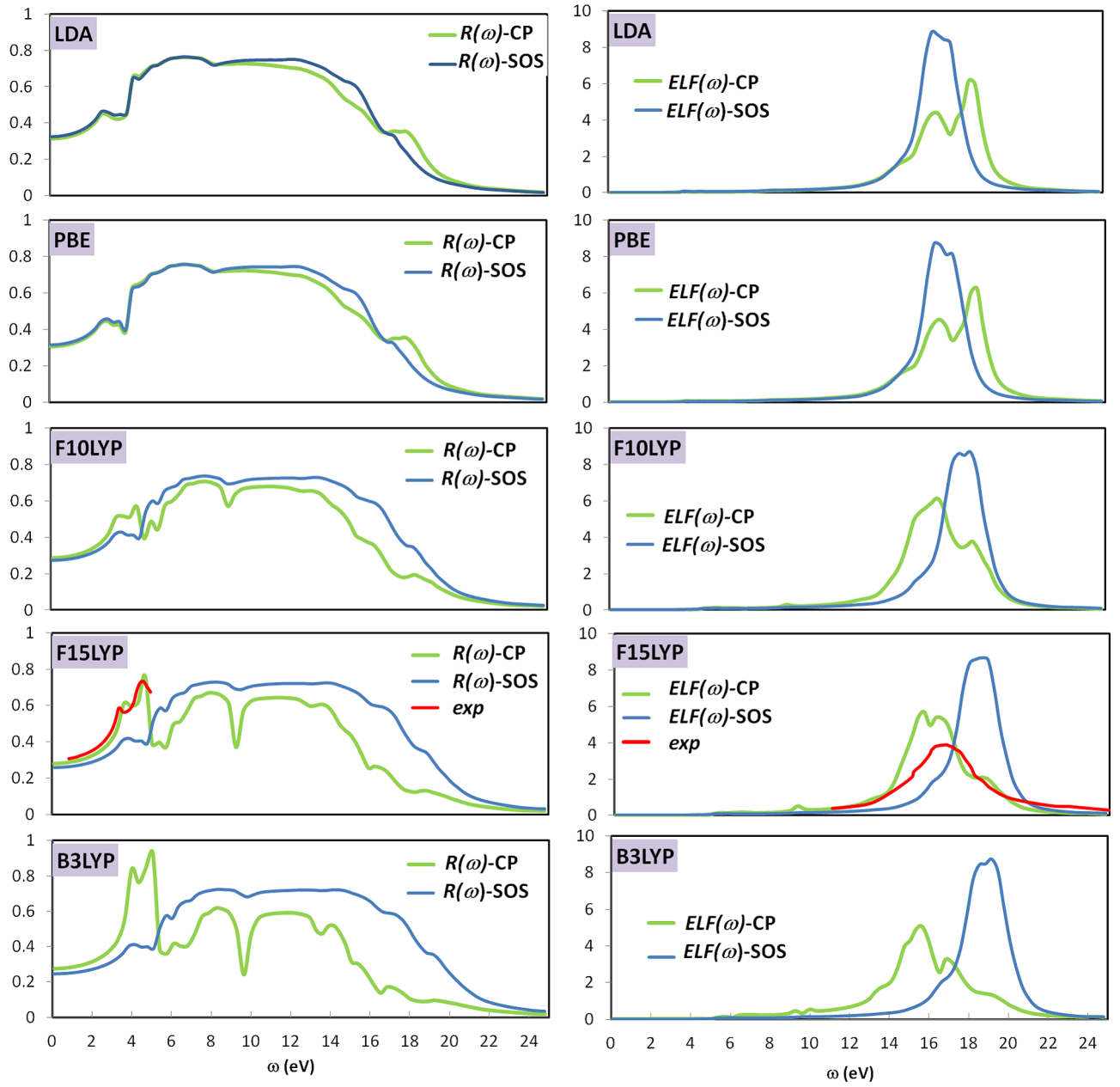

Figure 5. ELF(ω) and $R(\omega)$ of silicon computed with different functionals. IS = 36, T = (10,25) and η = 0.11 eV. Experimental data have been taken from refs 14 and 38.

that the approximation made on the imaginary part of the dielectric constant (eq 20) is satisfactory with this percentage of exchange (15%), whereas it is less satisfactory with F10LYP.

The region below E_g also has been analyzed. Much higher resolution is required to check for the presence of bound excitons below E_g. F15LYP highly resolved spectrum (IS = 150, η = 0.01 mHa) computed in a narrow region close to the band gap edge shows a first resonance downshifted with respect to E_g = 3.5234 eV by 0.5 meV. Thus, the optical spectrum below E_g shows the presence of a very weakly bound exciton.

Electron Energy Loss Function (ELF(ω)) and Reflectivity (R(ω)) Spectrum. ELF(ω) is the $\mathcal{I}_m(-1/\epsilon^{\infty}(\omega))$ function. It has a peak at $\mathcal{R}_e(\epsilon^{\infty}(\omega)) = 0$; the corresponding frequency is the plasmon pole (ω_p). It describes the collective harmonic oscillations of electrons, with respect to the fixed lattice of ions. Above the plasmon frequency, the external field oscillates too quickly for the electrons to follow and a material loses its reflectivity ($R(\omega)$) dramatically, where $R(\omega)$ is defined as

$$R(w) = \left| \frac{1 - \sqrt{\epsilon^{\infty}(\omega)}}{1 + \sqrt{\epsilon^{\infty}(\omega)}} \right|^2$$

The calculated ELF corresponds to the intensity in the electron energy loss spectroscopy analysis (low valence energy) for which the wavelength of the field is still very large, compared to the size of a unit cell (wavelength vector modulus $q \simeq 0$). As for the UV spectrum, we analyze now the effect of the computational setup on the computed ELF(ω) and $R(\omega)$ spectra.

- Computational parameters. ELF(ω) and $R(\omega)$ spectra computed with several selections of T and IS parameters have been reported in Figure 4. ELF(ω) and $R(\omega)$ spectra computed

DOI: 10.1021/acs.jctc.5b00199
J. Chem. Theory Comput. XXXX, XXX, XXX−XXX

Table 1. Electronic Direct Gap, Coupled Perturbed Static (High-Frequency) Dielectric Constant, and Plasmon Energy of Si, SiC, and LiF

	PBE	F10LYP	F15LYP	B3LYP	F40LYP	F50LYP	expt
Si							
gap (eV)	2.57	3.24	3.52	3.77			3.4 (ref 52)
ϵ^{∞}	11.6	11.2	10.6	10.2			11.8 (ref 53)
plasmon (eV)	16.3	16.3	15.5	15.3			16.8 (ref 38)
SiC							
gap (eV)	4.49	5.47	5.87	6.26			6.0 (refs 54−56)
ϵ^{∞}	6.8	6.7	6.4	6.3			6.5 (ref 57)
plasmon (eV)	21.9	21.7	21.6	20.8			22.2 (ref 42)
LiF							
gap (eV)	9.15	10.42	11.03	11.78	14.21	15.27	14.1 (ref 43)
ϵ^{∞}	2.0	1.9	1.9	1.8	1.8	1.7	1.9 (ref 58)
plasmon (eV)	24.4	24.4	24.6	25.3	25.7	25.9	24.9 (refs 44, 46), 25.7 (ref 47)

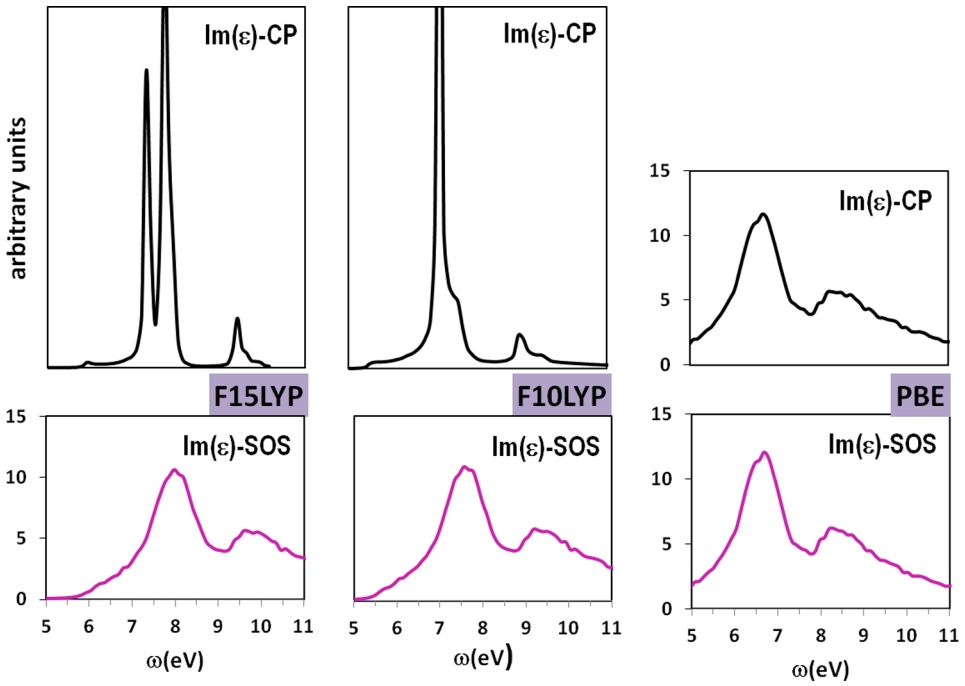

Figure 6. UV spectrum of SiC at various levels of theory. IS = 36, T = (8,25), and η = 0.055 eV.

with several selections of T and IS parameters have been reported in Figure 4. The effect of integral tolerance parameters controlling the exchange series has been analyzed by considering increasing values of T, T = (8,15), (8,25), and (8,35) (the truncation of the Coulomb series has been shown to affect the spectra is a minor way; see Figure 1). The shape of both ELF(ω) and $R(\omega)$ spectra over the entire 0−25 eV energy range is marginally affected by the selection of T; variations of the absolute intensities are particularly visible in the low-frequency region, which, however, turn out to be negligible when considering the T = (8,25) and T = (8,35) spectra. The ELF seems to be quite stable, with respect to the **k** sampling: only in the case of the poorest **k** mesh here adopted, IS = 16, the ELF peak appears noisy, even if ω_p is correctly predicted, with respect to the IS = 36 reference.

• The DFT functionals. SOS and SC-CP ELF(ω) and $R(\omega)$ spectra computed with several DFT functionals are reported in Figure 5. We first consider ELF(ω)-SOS. The value of ω_p is 16.4, 18.2, 17.5, 18.1, and 18.6 eV for LDA, PBE, F10LYP, F15LYP, and B3LYP, respectively. All the plasmon pole frequencies are shifted when SC-CP calculations are performed to ω_p = 18.1, 16.3, 16.3, 15.6, and 15.3 eV, respectively. With respect to the SOS counterpart, in SC-CP calculations, all functionals behave in a similar way: (i) they do not dramatically alter the shape of the ELF peak (it becomes less smooth with the appearance of shoulders that, in some cases, move to form a second peak); (ii) they shift ω_p. The plasmon energy is very sensitive to the rather flat plot of the real part of the dielectric constant when it crosses the frequency axis, and shoulders in the plot of ELF(ω) are related to oscillations in $\mathcal{R}_e(\epsilon^{\infty})$, as illustrated in Figure S2 in the ESI, where $\mathcal{R}_e(\epsilon^{\infty})$ is depicted in a narrow region close to ϵ^{∞} = 0.

We consider now $R(\omega)$. LDA and PBE SC−CP spectra are actually indistinguishable, with respect to the corresponding SOS ones. With hybrid functional $R(\omega)$-CP spectra, more structure is acquired, especially in the 3−7 eV region. We can also recognize a drop in R, in correspondence to the plasmon pole of ELF.

Computed ELF(ω) and $R(\omega)$ have been compared with the available experimental data. With regard to ELF, we can

DOI: 10.1021/acs.jctc.5b00199
J. Chem. Theory Comput. XXXX, XXX, XXX−XXX

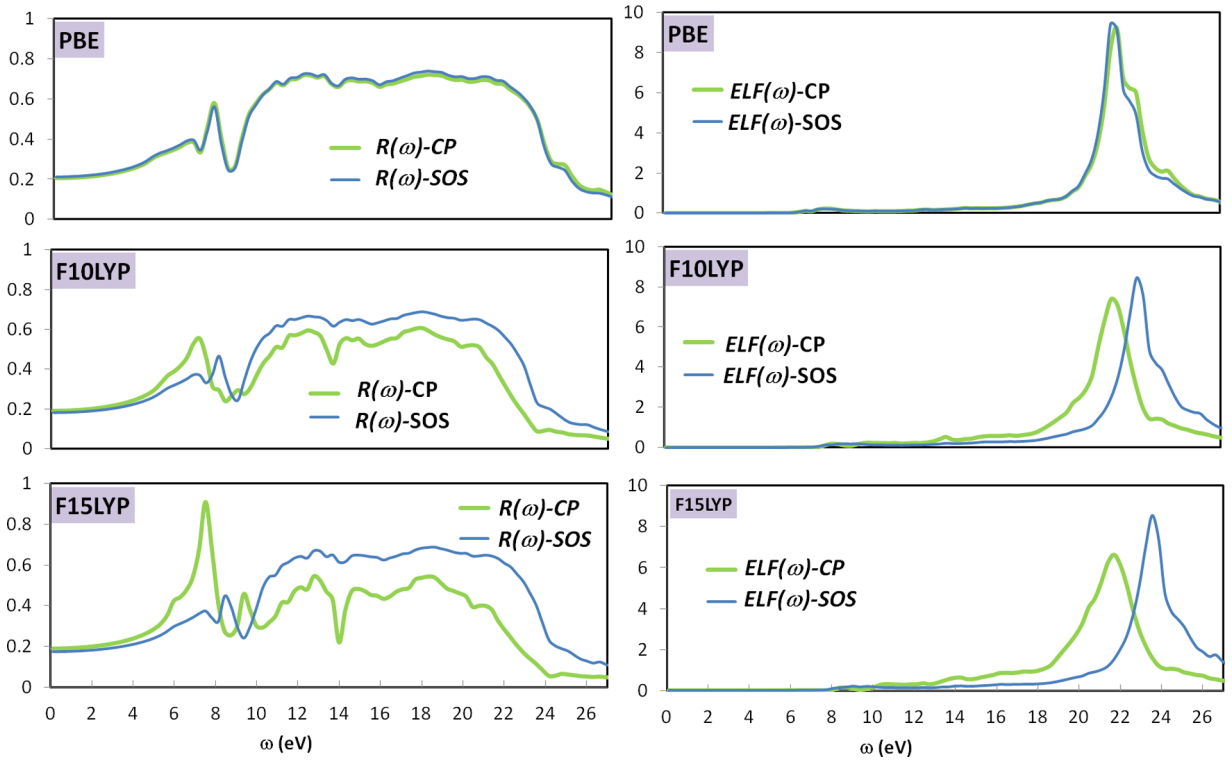

Figure 7. ELF(ω) and $R(\omega)$ of SiC: effect of the coupling at various levels of theory. IS = 36, T = (8,25) and η = 0.11 eV. Experimental data from ref 41

underline the good estimate of ω_p provided by PBE and F10LYP (the experimental value is 16.8 eV[38]); however, with PBE, the plasmon energy corresponds to the less intense peak in the ELF(ω) spectrum, whereas it is related to the main peak in the F10LYP case (see Figure 5).

A relatively good agreement with the experiment (ref 39) is obtained for $R(\omega)$: looking at the F10LYP spectrum, we can identify a doublet in the 3.5−4 eV region ($R \geq 50\%$) and a peak at 5 eV (R = 55%) before the principal one obtained at 7 eV (R = 75%), while the experimental plot of R shows a first peak at 3.4 eV ($R \simeq 60\%$), the largest one at 4.6 eV ($R \geq 75\%$) and the beginning of a diffuse one at 7 eV ($R \leq 70\%$). The relative intensities are not perfectly reproduced in our calculation, with respect to the good experimental resolution in this range of energy; however, the overall shape is very similar. In particular, we obtain R = 30% as observed in the experiment for $h\nu \leq 1$ eV.

SiC. The cubic (3C) polytype of SiC ($F\bar{4}3m$ space group) is a wide-gap semiconductor with a static dielectric constant twice as small as that of silicon (see Table 1), and an expected larger electron−hole interaction. The electronic structure, band structure (BS), and projected density of states (PDOS) are resumed in Figure S3 and Table S1 in the ESI.

SiC has an indirect band gap $E_g(\Gamma \rightarrow X)$ at 2.54 eV, a direct band gap in X, $E_g(X)$ = 5.87 eV (F15LYP). The gaps computed at the other special **k** points are considerably larger: $E_g(L)$ = 7.50 eV, $E_g(\Gamma)$ = 7.21 eV, and $E_g(U(X))$ = 7.13 eV; the $E_{\mathrm{HOMO}\rightarrow\mathrm{LUMO+1}}(\Gamma)$ = 8.26 eV is the other lowest energy difference between the VB and CB bands, followed by $E_{\mathrm{HOMO}\rightarrow\mathrm{LUMO+1}}(X, L)$ = 9.54, 9.60 eV (see Table S1 in the ESI).

The UV spectrum computed with the F10LYP and F15LYP functionals is reported in Figure 6. The F15LYP UV spectrum is dominated by the presence of two very intense peaks at 7.2 and 7.9 eV and small ones at 5.9, 9.2, and 9.5 eV. The analysis of the SiC band structure (see Figure S2 and Table S1 in the ESI) permits the following attributions: the lowest peak comes from HOMO → LUMO transitions in the vicinity of the minimum direct gap; the high peaks at 7.3 and 7.9 eV from HOMO → LUMO transitions, close to the L point for the former and along the $\Gamma-K-W$ line for the latter; the peak at 9.2 eV to HOMO → LUMO+1 transitions along the $\Gamma-L$ line and the 9.5 eV to HOMO → LUMO+1 transitions close to X. Several experimental studies[40,41] have analyzed the structure of $\mathcal{I}_m(\epsilon)$, by identifying peaks at 5.96, 7.43, 7.73, 9.03, and 9.4 eV. Positions and assignments of the computed peaks are, therefore, in agreement with observations (see ref 41). The F15LYP computed spectrum reproduces the experimental one quite nicely, although slightly shifted toward lower energies (by ∼0.1−0.2 eV) (see Figure 3); rather unsatisfactory is, instead, the F10LYP one, because of a reversed ratio between the intensities of the two main peaks and a smoother shape close to the band gap edge (Figures 3 and 6).

The presence of a very weak bound exciton has been also found: the highly resolved F15LYP spectrum (IS = 150, η = 0.01 mHa) computed in a narrow region close to the band gap edge shows a first resonance downshifted with respect to E_g = 5.873 eV by 2.0 meV.

$R(\omega)$ and ELF(ω) CP and SOS spectra computed with PBE, F10LYP and F15LYP are reported in Figure 7. A good agreement with the experiment[42] is obtained for the PBE and F10LYP plasmon energies, at 21.7 and 21.9 eV, respectively (see Table 1).

For R, a value of 20% is obtained at low energy ($h\nu \leq 1$ eV), in good agreement with the experimental datas of Logothetidis and Petalas.[40] A shoulder at ∼6 eV ($R \simeq 40\%$) and a peak at 7−8 eV ($R \leq 60\%$ with PBE and F10LYP, $R > 80\%$ with F15LYP)

DOI: 10.1021/acs.jctc.5b00199
J. Chem. Theory Comput. XXXX, XXX, XXX−XXX

are found with the coupled-perturbed calculation, also in agreement with the latter reference (R = 40% at 6 eV and $R \simeq$ 60% at 7.8 eV). Above 12 eV, R is essentially constant and equal to ∼40%−50% up to 18 eV (CP-F15LYP), before decreasing to zero at higher energy. No experimental data have been found for comparison in this energy range.

LiF. LiF has a rock-salt structure ($Fm\bar{3}m$ space group); ϵ^{∞} = 1.92 (see Table 1).

The electronic structure, band structure (BS), and projected density of states (PDOS) of LiF are shown in Figure S4 in the ESI. At the Γ-point, the gap ($E_g(\Gamma)$) is equal to 15.39, 14.07, and 11.61 eV for B3LYP, F40LYP, and F50LYP, respectively (see Table 1); the experimental gap is 14.1−14.2 eV,[43] which is close to the F40LYP value. The gaps in correspondence to other special **k**-points are as follows: $E_g(L)$ = 14.09, 16.61, and 17.95 eV for B3LYP, F40LYP, and F50LYP, respectively; $E_g(X)$ = 18.63, 21.34, and 22.81 eV for B3LYP, F40LYP, and F50LYP, respectively.

The SC-CP F50LYP UV spectrum (Figure 8) is characterized by an intense peak at 13.86 eV, which is 1.48 eV lower

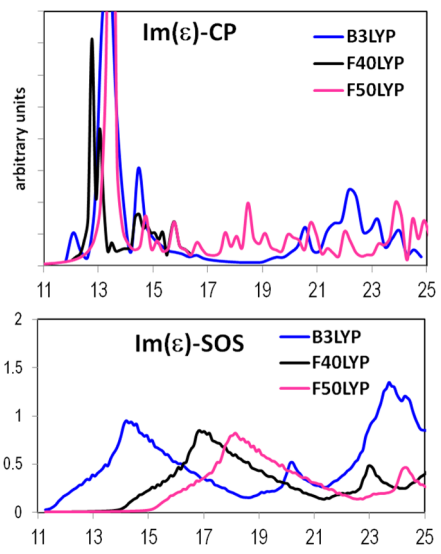

Figure 8. UV spectrum of LiF at various levels of theory. IS = 16, T = (8,25), and η = 0.055 eV.

than $E_g(\Gamma)$: it is due to bound excitons originated from HOMO → LUMO transitions in the vicinity of the minimum direct gap; from 15 eV to 25 eV, the spectrum is characterized by interband transitions from oscillators localized in a wide region along the Γ−L−X path (see Figure S3 in the ESI. By comparing the computed spectrum with the experimental spectrum (refs 44 and 45), we see that, although the overall shape is well reproduced, the calculated exciton peak is shifted to higher energy (the experimental peak is at 12.6 eV) (see Figure 3). With F40LYP, the exciton is at 12.85 eV, shifted with respect to $E_g(\Gamma)$ by 1.25 eV and in fair agreement with the position of the observed one. Unlike F50LYP and F40LYP, the B3LYP spectrum appears unsatisfactory, because of the absence of the bound exciton: we see, indeed, a small peak at 12.01 eV and a more intense one at 13.5 eV, both at higher energy, with respect to the band gap ($E_g(\Gamma)$ = 11.61 eV).

$R(\omega)$ shows a first thin peak ($R \simeq$ 65%) in the exciton energy range at ∼12−14 eV and a wide one ($R \simeq$ 50%) in the region between 20 eV and 28 eV (see Figure 9). Both signals are experimentally observed: the former ($R \simeq$ 50%) at 11 eV and the latter ($R \simeq$ 40%) centered at 23 eV (see refs 44 and 45).

ELF(ω) spectra are reported in Figure 9. In all spectra, we can recognize small losses in the exciton region and a wide intense one at ∼25 eV, because of the plasmon resonance of the valence electrons. The plasmon energies are at 25.3, 25.7, and 25.9 eV for B3LYP, F40LYP, and F50LYP, respectively, in good agreement with the experimental value, ω_p = 24.9 eV,[45,46] and ω_p = 25.7 eV.[47]

DISCUSSION

$\mathcal{I}_m(\epsilon^{\infty})$ computed with the SC-CP procedure correctly reproduces the experimental UV spectrum and properly describes the observed excitons, weakly bound in Si and SiC, strongly bound in LiF. In the SC-CP scheme, crystalline orbitals can relax in response to an electric field perturbation and excitons appear. Relaxation is ruled by the coupling matrices U, that, in turn, are dependent on the $B_{ia,\mathbf{k}}^{ia(ai),\mathbf{k}}$ integrals. This leads to a resonance frequency that is shifted with respect to the vertical transition $i_{\mathbf{k}} \rightarrow a_{\mathbf{k}}$ by the real quantity $B_{ia,\mathbf{k}}^{ia,\mathbf{k}} = 2\langle i_{\mathbf{k}} a_{\mathbf{k}} | a_{\mathbf{k}} i_{\mathbf{k}} \rangle - \langle i_{\mathbf{k}} a_{\mathbf{k}} | i_{\mathbf{k}} a_{\mathbf{k}} \rangle$. Thus, in a certain region of the **k**-space, generally in correspondence to a critical point, there may be an accumulation of oscillators resonating in a narrow energy range and whose strengths sum up. The result is the presence in the UV spectrum of new intense peaks (excitons) which are not observed in the SOS analogue. The number of oscillators $\rho(\omega_{ia,\mathbf{k}})$ resonating approximately at $\omega_{ia,\mathbf{k}} \pm \eta$ is dependent on the DOS shape of the valence and conduction bands: if the latter ones are thin as in molecular systems (or for **k**-point where the effective mass is large), the density of transition states at the gap, multiplied by η, will be equal to one, since there is only the $i_{\mathbf{k}} \rightarrow a_{\mathbf{k}}$ transition in the energy range $\omega_{ia,\mathbf{k}} \pm \eta$ (**k** = **0** for the molecule), and the shift of the pole will be as large as $B_{ia,\mathbf{k}}^{ia,\mathbf{k}}$. In contrast, for semiconductors with a small effective mass at the gap, $\rho(\omega_{ia,\mathbf{k}})$ is small and the pole is not expected to be greatly shifted. However, for photon energies larger than the gap and corresponding to transition energies between the VB and CB states belonging to the DOS maxima, the shift is the largest one. In other words, the shape of the UV-vis spectrum can change when the coupling is taken into account, even if the gap (lowest transition energy) is unshifted. Nevertheless, the appearance of excitons in the UV spectrum is observed only when a certain amount of exact exchange is incorporated in the DFT functionals, whereas with pure DFT $\mathcal{I}_m(\epsilon^{\infty})$-CP and $\mathcal{I}_m(\epsilon^{\infty})$-SOS practically coincide. An explanation for this behavior is that the integral, $2\langle i_{\mathbf{k}}(1)\ a_{\mathbf{k}}(2)|1/r_{12}|\ a_{\mathbf{k}}(1)\ i_{\mathbf{k}}(2)\rangle$, the Coulomb term of $B_{ia,\mathbf{k}}^{ia,\mathbf{k}}$, is probably relatively small, with respect to the integral $\langle i_{\mathbf{k}}(1)\ a_{\mathbf{k}}(2)|1/r_{12}|i_{\mathbf{k}}(1)\ a_{\mathbf{k}}(2)\rangle$, the HF exchange potential of $B_{ia,\mathbf{k}}^{ia,\mathbf{k}}$. In the "Coulomb term": $\langle i_{\mathbf{k}}(1)\ a_{\mathbf{k}}(2)|1/r_{12}|a_{\mathbf{k}}(1)\ i_{\mathbf{k}}(2)\rangle$ (as well as in $B_{ia,\mathbf{k}}^{ai,\mathbf{k}}$), electron (1) belongs to different and orthogonal $i_{\mathbf{k}}(1)$- and $a_{\mathbf{k}}(1)$-orbitals, leading to a small value of the integral (at long distance r_{12}). In contrast, the "exchange term" represents the average repulsion $1/r_{12}$ between the hole $i_{\mathbf{k}}^2(1)$ and electron $a_{\mathbf{k}}^2(2)$ densities. This is the reason why the energy shift of the pole is generally negative, as shown in the section entitled "Applications", when using HF or hybrid DFT Hamiltonians ($B_{ia,\mathbf{k}}^{ia,\mathbf{k}}$ is negative and a pole appears before the transition energy: $\omega_{ia,\mathbf{k}} < \epsilon_{a_{\mathbf{k}}}^{(0)} - \epsilon_{i_{\mathbf{k}}}^{(0)}$). In DFT, the integrals $\langle i_{\mathbf{k}} a_{\mathbf{k}} | i_{\mathbf{k}} a_{\mathbf{k}} \rangle$ coming from the HF exchange potential is missing and replaced by integrals similar to the "Coulomb term" multiplied by the derivative of the exchange-correlation functional of the electron

DOI: 10.1021/acs.jctc.5b00199
J. Chem. Theory Comput. XXXX, XXX, XXX−XXX

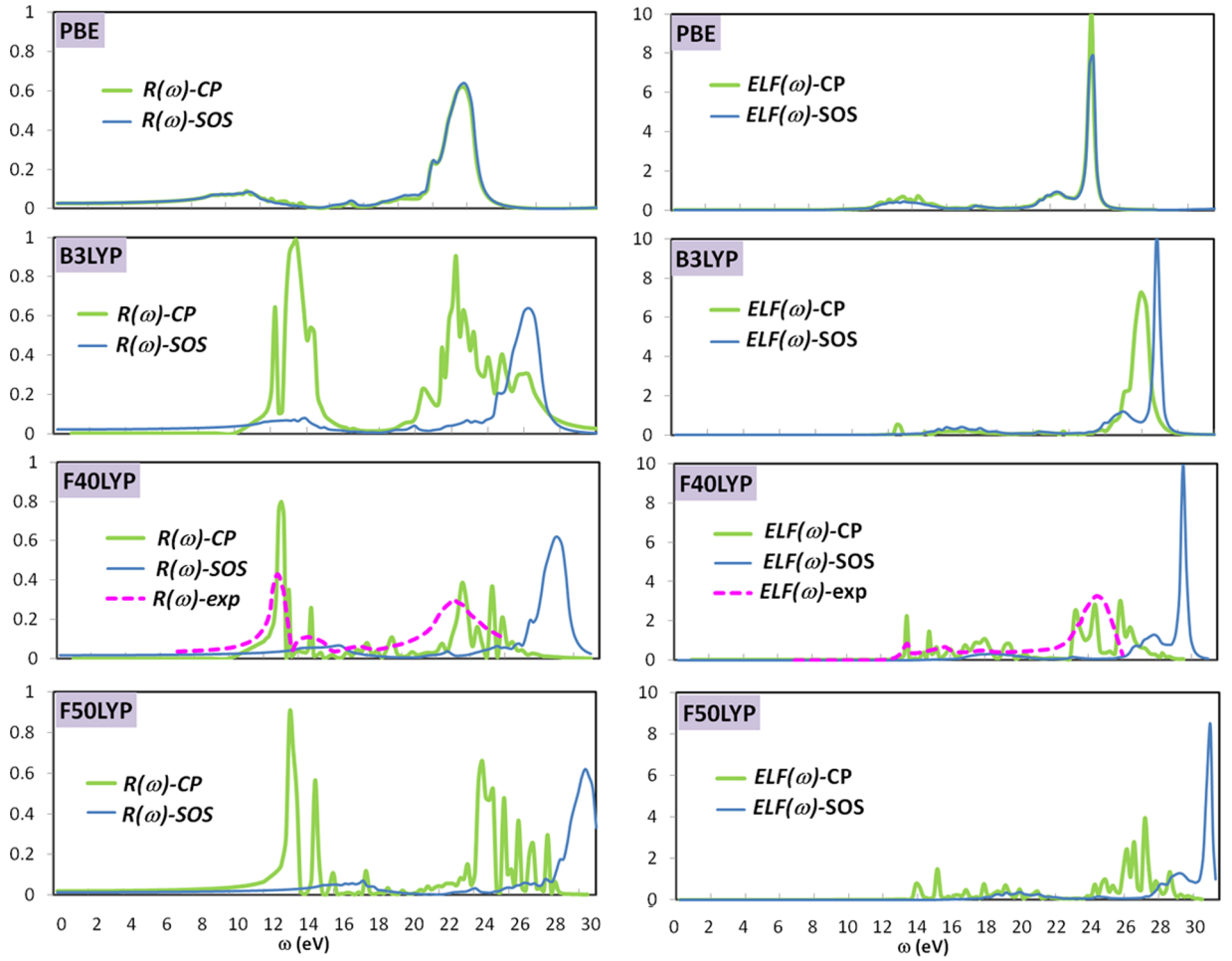

Figure 9. ELF(ω) and $R(\omega)$ of LiF at various levels of theory. IS = 16, T = (8,15), and η = 0.11 eV. Experimental data from ref 45.

density (and its gradient), with respect to the field.[5,24] The orbital relaxation effect in the presence of a frequency-dependent field near resonances then is weak: there is no shift of the energy ($B^{ia,k}_{ia,k} = 2\langle i_k a_k | a_k i_k \rangle \simeq 0$), and the lowest excitation energy is equal to the direct band gap, as has also been shown in refs 24 and 25 for extended systems. In addition, "pure" DFT suffers for the self-interaction error, the spurious electrostatic interaction of an electron with itself. As a result, the electron is partly repelled from itself, leading to an asymptotic decay of the exchange-correlation potential that is too weak. Correction for the self-interaction error is necessary to properly describe the polarization of any system. It is partially embodied in the fraction of exact exchange in hybrids DFT, thus partially recovering the correct asymptotic behavior of exchange-correlation potential.[25,48−50]

The necessity to use hybrids to calculate optical transitions has been generally recognized, although the best choice for the exchange-correlation functional is still debated. Conventional hybrids are not able to describe all excitons and especially those involving charge-transfer excitations. Several functional forms have been proposed in order to circumvent this problem and, among them, we mention the use of a tuned fraction of exact exchange in a conventional hybrid functional; the use of semiempirical conventional hybrid functionals that contain a large number of empirical parameters with the objective of providing a balanced treatment of main properties including long-range charge-transfer interactions; long-range corrected functionals with a fixed (even if empirically determined) long-range separation parameter; long-range separated functionals with system-specific optimal tuning to determine the range separation parameter (see refs 20 and 21, and references therein). Although this latter procedure has been successfully applied for the description of polarizability and band gaps in solids, no comprehensive applications to the calculations of the entire UV, ELF, and R spectra has been reported yet. Kresse and co-workers applied the HSE functionals (varying also the range separation parameter) to semiconductors and insulators: however, they were not able to satisfactorily describe the LiF absorption spectrum.[51] Therefore, we preferred to follow the former scheme that also appears to be particularly attractive, since it involves the use of conventional exchange functionals, whose performances have been well-assessed during decades of studies and applications. To this extent, in the spirit of the work of Marques et al.,[18] Skone et al.,[19] and Brothers et al.,[22] we found that a percentage of HF exchange corresponding to the inverse of the static optical dielectric constant, $1/\epsilon^{\infty}(0)$ (~10% for Si, 15%−20% for SiC, and 40%−50% for LiF), leads to band gaps and static dielectric constants that are in good agreement with the experiment. It also follows that the UV-vis absorption spectrum (position and relative intensity of the peaks) is also well-described with these percentage values, particularly for SiC (Figure 3). Slightly less straightforward is the case of Si for which the F10LYP functional, which is the best choice according to this procedure, does not give a UV spectrum as

DOI: 10.1021/acs.jctc.5b00199
J. Chem. Theory Comput. XXXX, XXX, XXX−XXX

good as the F15LYP functional. Also, in the case of LiF, we found a better result with F40LYP instead of F50LYP, which is the best choice according to this scheme. This finding is not surprising, since the procedure leads to a simple description of the screened electron repulsion in a medium by empirically tuning the amount of exact exchange with only one parameter (the inverse of the static dielectric constant of the crystal itself). The choice of this unique parameter may be questionable. In addition to this attempt to obtain a satisfactory description of a physical property (as the dielectric constant) by changing the amount of exact exchange can alter the delicate balance between exchange and correlation in ways that could be disadvantageous for other properties.

Nevertheless, our work shows that a fraction of exact exchange approximatively equal to the inverse of the static dielectric constant leads to UV spectra comparable with the experimental ones. If no shift of the CB is found for semiconductors such as Si and medium SiC, the relative intensity is enhanced at low transition energy after the electron gap. With regard to LiF, the "red" shift of the optical gap, with respect to the lowest vertical transition energy, increases as the percentage of HF exchange (x-value) increases in the SC-CP process. However, this is also the case of the opposite "blue" shift of the lowest vertical transition energy, so that there is no simple linear relationship between the optical gap value and x, as for Si and SiC, and more generally between the full spectrum (UV, ELF, and R) and the exchange percentage. Nevertheless, for the three studied compounds, the lowest energy peaks are enhanced by coupled hybrid methods with respect to SOS, leading to a shift of the entire absorption spectrum, as well as to a shift of ELF and R, toward low energies. With regard to the plasmon energy, its value is very sensitive to small amplitude oscillations of $\mathcal{R}_e(\epsilon^\infty)$ around zero; the ELF maximum can be shifted and shoulders appear. The origin of such oscillations comes from faked occupied to virtual vertical transitions that are not completely smoothed out by the SC-CP method. However, the ELF plasmon frequency is described relatively well when the percentage value of exchange is ∼10% for both Si and SiC crystals, and 40% for LiF. We have also shown that the band energy for which Si and SiC reflect the light (band energy where the reflectivity is not null) slightly decreases as the percentage of HF exchange increases, while the peak of R at low energy becomes larger. This result was previously found for the absorption spectrum and showing that the SC-CP method involving virtual orbitals (as SCF occupied ones) in the optimization process leads to the decrease of the conduction bandwidth. Virtual unrelaxed orbitals, which can have very large unphysical eigenvalues, finally do not contribute to the spectrum anymore, or at much lower energy than their eigenvalues, when they are included in the SC-CP process.

CONCLUSIONS

In this work, the frequency-dependent coupled-perturbed method already implemented in the CRYSTAL code, which uses localized atomic orbitals, has been extended in order to compute the real and imaginary parts of the dielectric response property of periodic systems in the entire UV-vis range of energy. The use of the vectorial epsilon-algorithm has been essential to improve convergence of the SC-CP process near resonances. The method allows one to obtain numerically both the poles and oscillator strengths of the electronic spectrum from the dielectric reponse property without storing large Hamiltonian matrices to be diagonalized.

The percentage of Hartree−Fock exchange in the Hamiltonian (with 100% HF exchange, the method is equivalent to TDHF, with 0% to TDDFT) is easily modified, and its influence on the UV-vis absorption spectrum, electron loss function, and reflectivity is explored.

In this first application of the CRYSTAL code to the study of the excited states of solids, we employed the well-known B3LYP hybrid functional: we have found that incorporating a percentage of HF exchange corresponding to the inverse of the static optical dielectric constant, $1/\epsilon^\infty(0)$, in the functional (used in refs 18 and 19, to obtain band gaps in good agreement with experiment), also leads to satisfactory UV-vis absorption spectra (position and relative intensity of the peaks). Delocalized, weakly bound excitons as in Si, and localized, strongly bound ones as in LiF, are both correctly described with this approach. The electron loss function and reflectivity computed by roughly employing the same amount of HF exchange are also in good agreement with the experiments.

ASSOCIATED CONTENT

Supporting Information

Details about electron structures (DOS and band structures), together with plots of $\mathcal{R}_e(\epsilon^\infty)$ in a narrow region close to ϵ^∞ = 0 are provided as Supporting Information. The Supporting Information is available free of charge on the ACS Publications website at DOI: 10.1021/acs.jctc.5b00199.

AUTHOR INFORMATION

Corresponding Author

*E-mail: anna.ferrari@unito.it.

Notes

The authors declare no competing financial interest.

ACKNOWLEDGMENTS

The authors are grateful to Prof. R. Dovesi for their kind help and fruitful suggestions. A.M.F. acknowledges CINECA (Iscra Project B HOME) for computational resources.

REFERENCES

(1) Hurst, G.; Dupuis, M.; Clementi, E. *Ab Initio* Analytic Polarizability, First and Second Hyperpolarizabilities of Large Conjugated Organic Molecules: Applications to Polyenes C_4H_6 to $C_{22}H_{24}$. *J. Chem. Phys.* **1988**, *89*, 385−395.

(2) Ferrero, M.; Rérat, M.; Orlando, R.; Dovesi, R. The Calculation of Static Polarizabilities of 1−3D Periodic Compounds. the Implementation in the Crystal Code. *J. Comput. Chem.* **2008**, *29*, 1450−1459.

(3) Dovesi, R.; Saunders, V. R.; Roetti, C.; Orlando, R.; Zicovich-Wilson, C. M.; Pascale, F.; Civalleri, B.; Doll, K.; Harrison, N. M.; Bush, I. J. et al.*CRYSTAL14 User's Manual*; University of Torino: Torino, Italy, 2014.

(4) Dovesi, R.; Orlando, R.; Zicovich-Wilson, C. M.; Civalleri, B.; Maschio, L.; Erba, A.; Casassa, S.; Ferrabone, M.; Pierre, M. D. L.; D'Arco, P.; et al. CRYSTAL14: A Program for the *Ab Initio* Investigation of Crystalline Solids. *Int. J. Quantum Chem.* **2014**, *114*, 1287−1317.

(5) Ferrero, M.; Rérat, M.; Orlando, R.; Dovesi, R.; Bush, I. J. Coupled Perturbed Kohn−Sham Calculations of Static Polarizabilities of Periodic Compounds. *J. Phys. Conf. Ser.* **2008**, *117*, 12016.

(6) Bernasconi, L.; Tomić, S.; Ferrero, M.; Rérat, M.; Orlando, R.; Dovesi, R.; Harrison, N. M. First-Principles Optical Response of Semiconductors and Oxide Materials. *Phys. Rev. B* **2011**, *83*, 195325.

DOI: 10.1021/acs.jctc.5b00199
J. Chem. Theory Comput. XXXX, XXX, XXX−XXX

(7) Erba, A.; Dovesi, R. Photoelasticity of Crystals from Theoretical Simulations. *Phys. Rev. B* **2013**, *88*, 045121-1−045121-8.
(8) Mahmoud, A.; Erba, A.; El-Kelany, K. E.; Rérat, M.; Orlando, R. Low-Temperature Phase of $BaTiO_3$: Piezoelectric, Dielectric, Elastic, and Photoelastic Properties from *Ab Initio* Simulations. *Phys. Rev. B* **2014**, *89*, 045103-1−045103-9.
(9) Karna, S. P.; Dupuis, M. Frequency Dependent Nonlinear Optical Properties of Molecules: Formulation and Implementation in the HONDO program. *J. Comput. Chem.* **1991**, *12*, 487−504.
(10) Lorenz, M.; Usvyat, D.; Schütz, M. Local *Ab Initio* Methods for Calculating Optical Band Gaps in Periodic Systems. I. Periodic Density Fitted Local Configuration Interaction Singles Method for Polymers. *J. Chem. Phys.* **2011**, *134*, 094101-1−094101-14.
(11) Lorenz, M.; Maschio, L.; Schütz, M.; Usvyat, D. Local *Ab Initio* Methods for Calculating Optical Band Gaps in Periodic Systems. II. Periodic Density Fitted Local Configuration Interaction Singles Method for Solids. *J. Chem. Phys.* **2012**, *137*, 204119−204214.
(12) Olevano, V.; Reining, L. Excitonic Effects on the Silicon Plasmon Resonance. *Phys. Rev. Lett.* **2001**, *86*, 5962.
(13) Rohlfing, M.; Louie, S. G. Electron-Hole Excitations in Semiconductors and Insulators. *Phys. Rev. Lett.* **1998**, *81*, 2312−2315.
(14) Aspnes, D. E.; Studna, A. A. Dielectric functions and optical parameters of Si, Ge, GaP, GaAs, GaSb, InP, InAs, and InSb from 1.5 to 6.0 eV. *Phys. Rev. B* **1983**, *27*, 985−1009.
(15) Philipp, H. R.; Ehrenreich, H. Optical Properties of Semiconductors. *Phys. Rev.* **1963**, *129*, 1550−1560.
(16) Lautenschlager, P.; Garriga, M.; Cardona, M. Temperature Dependence of the Dielectric Function and Interband Critical Points in Silicon. *Phys. Rev. B* **1987**, *36*, 4821−4830.
(17) Onida, G.; Reining, L.; Rubio, A. Electronic Excitations: Density-Functional versus Many-Body GreenĂŹs-Function Approaches. *Rev. Mod. Phys.* **2002**, *74*, 601−659.
(18) Marques, M. A. L.; Vidal, J.; Oliveira, M. J. T.; Reining, L.; Botti, S. Density-Based Mixing Parameter for Hybrid Functionals. *Phys. Rev. B* **2011**, *83*, 035119-1−035119-5.
(19) Skone, J. H.; Govoni, M.; Galli, G. Self-Consistent Hybrid Functional for Condensed Systems. *Phys. Rev. B* **2014**, *89*, 195112-1−195112-12.
(20) Kronik, L.; Stein, T.; Refaely-Abramson, S.; Baer, R. Excitation Gaps of Finite-Sized Systems from Optimally Tuned Range-Separated Hybrid Functionals. *J. Chem. Theory Comput.* **2012**, *8*, 1515−1531.
(21) Eisenberg, H. R.; Baer, R. A New Generalized Kohn−Sham Method for Fundamental Band-Gaps in Solids. *Phys. Chem. Chem. Phys.* **2009**, *11*, 4674−4680.
(22) Brothers, E. N.; Izmaylov, A. F.; Scuseria, G. E.; Kudin, K. N. Analytically Calculated Polarizability of Carbon Nanotubes: Single Wall, Coaxial, and Bundled Systems. *J. Phys. Chem. C* **2008**, *112*, 1396−1400.
(23) Izmaylov, A. F.; Brothers, E. N.; Scuseria, G. E. Linear-scaling calculation of static and dynamic polarizabilities in Hartree-Fock and density functional theory for periodic systems. *J. Chem. Phys.* **2006**, *125*, 224105−9.
(24) Izmaylov, A. F.; Scuseria, G. E. Why are Time-Dependent Density Functional Theory Excitations in Solids Equal to Band Structure Energy Gaps for Semilocal Functionals, and How Does Nonlocal Hartree-Fock-type Exchange Introduce Excitonic Effects? *J. Chem. Phys.* **2008**, *129*, 034101.
(25) Hirata, S.; Head-Gordon, M.; Bartlett, R. J. Configuration Interaction Singles, Time-Dependent Hartree-Fock, and Time-Dependent Density Functional Theory for the Electronic Excited States of Extended Systems. *J. Chem. Phys.* **1999**, *111*, 10774.
(26) Otto, P. Calculation of the Polarizability and Hyperpolarizabilities of Periodic Quasi-one-dimensional Systems. *Phys. Rev. B* **1992**, *45*, 10876−10885.
(27) Rérat, M.; Ferrero, M.; Amzallag, E.; Baraille, I.; Dovesi, R. Comparison of the Polarizability of Periodic Systems Computed by Using the Length and Velocity Operators. *J. Phys. Conf. Ser.* **2008**, *117*, 012023.
(28) Rice, J. E.; Amos, R. D.; Colwell, S. M.; Handy, N. C.; Sanz, J. Frequency Dependent Hyperpolarizabilities with Application to Formaldehyde and Methyl Fluoride. *J. Chem. Phys.* **1990**, *93*, 8828−8839.
(29) Dirac, P. A. M. Note on Exchange Phenomena in the Thomas−Fermi Atom. *Proc. Cambridge Philos. Soc.* **1930**, *26*, 376.
(30) Vosko, S. H.; Wilk, L.; Nusair, N. Accurate Spin-Dependent Electron Liquid Correlation Energies for Local Spin Density Calculations: A Critical Analysis. *Can. J. Phys.* **1980**, *58*, 1200.
(31) Perdew, J. P.; Burke, K.; Ernzehof, M. Generalized Gradient Approximation Made Simple. *Phys. Rev. Lett.* **1996**, *77*, 3865−3868.
(32) Becke, A. D. Density-Functional Exchange-Energy Approximation with Correct Asymptotic Behavior. *Phys. Rev. A* **1988**, *38*, 3098−3100.
(33) Lee, C.; Yang, W.; Parr, R. G. Development of the Colle−Salvetti Correlation-Energy Formula into a Functional of the Electron Density. *Phys. Rev. B* **1988**, *37*, 785−789.
(34) CRYSTAL14 website (http://www.crystal.unito.it/basis-sets.php).
(35) Durand, E. *Solutions Numériques des Equations Algébriques, I&II*; Masson: Paris, 1960.
(36) Wynn, P. Acceleration Techniques for Iterated Vector and Matrix Problems. *Math. Comput.* **1962**, *16*, 301−322.
(37) Brezinski, C. Some Results and Applications Abouts the Vector ϵ-Algorithm. *J. Math.* **1974**, *4*, 335.
(38) Siebling, J. Optische Eigenschaften des Einkristallinen Siliziums aus Elektronenenergieverlustmessungen. *Z. Phys. B* **1978**, *31*, 355.
(39) Green, M. A. Self-Consistent Optical Parameters of Intrinsic Silicon at 300 K Including Temperature Coefficients. *Sol. Energy Mater. Sol. Cells* **2008**, *92*, 1305.
(40) Logothetidis, S.; Petalas, J. Dielectric Function and Reflectivity of 3C-Silicon Carbide and the Component Perpendicular to the *c* Axis of 6H-Silicon Carbide in the Energy Region 1.5−9.5 eV. *J. Appl. Phys.* **1996**, *80*, 1768.
(41) Theodorou, G.; Tsegas, G.; Kaxiras, E. Theory of Electronic and Optical Properties of 3C-SiC. *J. Appl. Phys.* **1999**, *85*, 2179.
(42) Heidt, A.; Chen, T.; Finger, F.; Rau, U.; Mayer, J.; Luysberg, M. Structure and Electronic Properties of μc-SiC:H for Photovoltaic Applications. *J. Phys. Conf. Series* **2011**, *326*, 012019.
(43) Kunz, A. B. Study of the Electronic Structure of Twelve Alkali Halide Crystals. *Phys. Rev. B* **1982**, *26*, 2056.
(44) Roessler, D. M.; Walker, W. C. Electronic Spectrum of Crystalline Lithium Fluoride. *J. Phys. Chem. Solids* **1967**, *28*, 1507−1515.
(45) Roessler, D. M.; Walker, W. C. Optical Constants of Magnesium Oxide and Lithium Fluoride in the Far Ultraviolet. *J. Opt. Soc. Am.* **1967**, *57*, 835−836.
(46) Caliebe, W. A.; Soininen, J. A.; Shirley, E. L.; Kao, C.-C.; Hamalainen, K. *Phys. Rev. Lett.* **2004**, *84*, 3907−3910.
(47) Creuzburg, M. Energieverlustspektren der Alkalihalogenide und der Metalle Cu, Ag und Au und Vergleich mit Optischen Messungen. *Z. Phys.* **1966**, *196*, 433.
(48) Perdew, J. P.; Zunger, A. Self-Interaction Correction to Density-Functional Approximations for Many-Electron Systems. *Phys. Rev. B* **1981**, *23*, 5048−5079.
(49) Pemmaraju, C. D.; Sanvito, S.; Burke, K. Polarizability of molecular chains: A self-interaction correction approach. *Phys. Rev. B* **2008**, *77*, 121204(R)-1−121204(R)-4.
(50) van Leeuwen, R.; Baerends, E. J. Exchange-Correlation Potential with Correct Asymptotic Behavior. *Phys. Rev. A* **1994**, *49*, 2421−2431.
(51) Paier, J.; Marsman, M.; Kresse, G. Dielectric Properties and Excitons for Extended Systems from Hybrid Functionals. *Phys. Rev. B* **2008**, *78*, 121201(R)-1−121201(R)-4.
(52) Zucca, R. R. L.; Shen, Y. R. Wavelength-Modulation Spectra of Some Semiconductors. *Phys. Rev. B* **1970**, *1*, 2668−2676.
(53) Weast, R. C. *Handbook of Chemistry and Physics*; CRC Press: Boca Raton, FL, 1989
(54) Dalven, R. Temperature Coefficient of the Energy Gap of β-Silicon Carbide. *J. Phys. Chem. Solids* **1965**, *26*, 439.

DOI: 10.1021/acs.jctc.5b00199
J. Chem. Theory Comput. XXXX, XXX, XXX−XXX

(55) Nishino, S.; Powell, J. A.; Will, H. A. Production of Large-Area Single-Crystal Wafers of Cubic SiC for Semiconductor Devices. *Appl. Phys. Lett.* **1983**, *42*, 460.
(56) Li, Y.; Lin-Chung, P. J. Band Structure and Electronic Properties of Native Defects in Cubic SiC. *Phys. Rev. B* **1987**, *36*, 1130−1135.
(57) Lyle, P.; Choyke, W. J. Static Dielectric Constant of SiC. *Phys. Rev. B* **1970**, *2*, 2255−2256.
(58) Burstein, E.; Perkowitz, S.; Brodsk, M. H. The Dielectric Properties of the Cubic IV−VI Compound Semiconductors. *J. Phys., Colloq. C4* **1968**, *29*, 78−83.

DOI: 10.1021/acs.jctc.5b00199
J. Chem. Theory Comput. XXXX, XXX, XXX−XXX